Loss of Indian Hedgehog Activates Multiple Aspects of a Wound Healing Response in the Mouse Intestine

WILLEMIJN A. VAN DOP,[*,‡,§] JAROM HEIJMANS,[*] NIKÈ V. J. A. BÜLLER,[*] SUSANNE A. SNOEK,[‖] SANNE L. ROSEKRANS,[*] ELISABETH A. WASSENBERG,[‡] MARIUS A. VAN DEN BERGH WEERMAN,[¶] BEATE LANSKE,[#] ALAN R. CLARKE,[**] DOUGLAS J. WINTON,[‡‡] MARK WIJGERDE,[§§] G. JOHAN OFFERHAUS,[‖‖] DAAN W. HOMMES,[*] JAMES C. HARDWICK,[*] WOUTER J. DE JONGE,[‖] IZAK BIEMOND,[*] and GIJS R. VAN DEN BRINK[*]

[*]Department of Gastroenterology and Hepatology, Leiden University Medical Center, Leiden, The Netherlands; [‡]Center for Experimental Molecular Medicine, [§]Department of Gastroenterology & Hepatology, [‖]Tytgat Institute for Liver and Intestinal Research, [¶]Department of Pathology, Academic Medical Center, Amsterdam, The Netherlands; [#]Department of Developmental Biology, Harvard School of Dental Medicine, Boston, Massachusetts; [**]School of Biosciences, University of Cardiff, Cardiff, United Kingdom; [‡‡]Cancer Research UK Department of Oncology, Cambridge Institute for Medical Research, Addenbrooke's Hospital, Cambridge, United Kingdom; [§§]Department of Reproduction and Development, Erasmus University Medical Center, Rotterdam, The Netherlands; and [‖‖]Department of Pathology, University Medical Center Utrecht, Utrecht, The Netherlands

BACKGROUND & AIMS: Indian Hedgehog (Ihh) is expressed by the differentiated epithelial cells of the small intestine and signals to the mesenchyme where it induces unidentified factors that negatively regulate intestinal epithelial precursor cell fate. Recently, genetic variants in the Hh pathway have been linked to the development of inflammatory bowel disease. **METHODS:** We deleted *Ihh* from the small intestinal epithelium in adult mice using *Cyp1a1-Cre*$Ihh^{fl/fl}$ conditional *Ihh* mutant mice. Intestines were examined by immunohistochemistry, in situ hybridization, and real-time polymerase chain reaction. **RESULTS:** Deletion of *Ihh* from the intestinal epithelium initially resulted in a proliferative response of the intestinal epithelium with lengthening and fissioning of crypts and increased Wnt signaling. The epithelial proliferative response was associated with loss of bone morphogenetic protein and Activin signaling from the epithelium of the villus and crypts, respectively. At the same stage we observed a substantial influx of fibroblasts and macrophages into the villus core with increased mesenchymal transforming growth factor-β signaling and deposition of extracellular matrix proteins. Prolonged loss of Ihh resulted in progressive leukocyte infiltration of the crypt area, blunting and loss of villi, and the development of intestinal fibrosis. **CONCLUSIONS: Loss of Ihh initiates several events that are characteristic of an intestinal wound repair response. Prolonged loss resulted in progressive inflammation, mucosal damage, and the development of intestinal fibrosis. Ihh is a signal derived from the superficial epithelial cells that may act as a critical indicator of epithelial integrity.**

Keywords: Indian Hedgehog; Intestine; Regeneration; Inflammation.

Differentiated cells in rapidly renewing tissues such as epithelia of the skin and the gastrointestinal tract are in a dynamic equilibrium with precursor cells to balance the rate of proliferation with cell loss at the epithelial surface. The balance between input and output in homeostatic dynamic equilibria depends on the presence of negative feedback loops. The fate and proliferation of intestinal precursor cells is regulated by Wnt signaling. Indian Hedgehog (Ihh) is the major Hedgehog (Hh) expressed in the colon and it is secreted by the mature enterocytes at the top of the crypt. Treatment of rats with Hh inhibitor cyclopamine resulted in increased Wnt signaling and precursor cell proliferation whereas enterocyte differentiation was impaired.[1] In $Ihh^{-/-}$ mice we observed a failure of proliferating cells to differentiate and impaired crypt formation but these mice were not viable and died well before birth.[1] Inhibition of Hh signaling in the developing intestine by transgenic expression of Hh antagonist Hedgehog interacting protein (Hhip) similarly resulted in accumulation of proliferating cells, some in ectopic foci on the small intestinal villi, and increased Wnt signaling.[2] Conversely, conditional activation of Hh signaling in the adult intestine by inducible deletion of Hh binding receptor Patch 1 (Ptch1; which acts by repressing the Hh signaling receptor Smoothened) resulted in inhibition of Wnt signaling and depletion of precursor cells that underwent premature differentiation into the enterocyte lineage.[3] Thus, Hh signaling seems to act as a negative feedback signal that contributes to the dynamic equilibrium between epithelial precursor cells and enterocytes in the intestinal epithelium,

Abbreviations used in this paper: α-Sma, α-smooth muscle actin; Bmp, bone morphogenetic protein; BrdU, bromodeoxyuridine; Gli, glioma-associated oncogene; Hh, Hedgehog; Hhip, Hedgehog-interacting protein; HRP, horseradish peroxidase; Ihh, Indian hedgehog; Pai-1, plasminogen activator inhibitor-1; pSmad1,5,8, phosphorylated Smad 1, 5, and 8; pSmad2,3, pSmad2,3, phosphorylated Smad 2 and 3; Ptch1, Patched1; RT-PCR, reverse-transcription polymerase chain reaction; SSC, standard saline citrate; Tgfβ, transforming growth factor-β.

0016-5085/$36.00
doi:10.1053/j.gastro.2010.07.045

but several important questions remain. First, although a genetic loss-of-function experiment has been performed in the developing intestine[2] a genetic loss-of-function experiment in the fully developed adult intestine still needs to be performed. Second, although we were unable to detect Shh in the mouse intestine by in situ hybridization[3] it has been shown using a *Shh*$^{Green\ fluorescent\ protein}$ reporter mouse that low levels of Shh may be expressed by rare cells at the crypt base and thus the relative contribution of Shh and Ihh to Hh signaling in the adult intestine still needs to be addressed. Third, Hh signaling is exclusively from the epithelium to the mesenchyme[3,4] and the mesenchymal factors that negatively regulate precursor cells in response to Hh signaling still await identification. Hh signaling regulates the expression of bone morphogenetic proteins (Bmps) in the developing and adult intestine[1,3,5] and increased Hh signaling in the adult extends the range of Bmp signaling through Smads1, 5, and 8 from the top of the crypt toward the base of the crypt.[3] Because the Bmp pathway is not normally active at the base of the crypt it is unlikely that Bmps are the major negative regulators of Wnt signaling or precursor cell fate. Indeed, a transgenic mouse that overexpressed the Bmp antagonist noggin in the intestinal epithelium did not have a phenotype until 3 weeks after birth[6,7] and these mice develop hamartomas, polyps that are characterized by abnormal growth of the mesenchyme rather than the epithelium. Possible Hh-dependent expression of transforming growth factor-β (Tgfβs) or Activins, which signal through Smad2 and 3, has not been examined.

The role of Hh signaling in the intestine may extend beyond negative regulation of epithelial precursor cells because a hypomorphic mutant of downstream transcription factor *GLI1* has now been linked to the development of inflammatory bowel disease.[8] Here we examine the role of Ihh signaling in the adult small intestine using mice in which *Ihh* can be conditionally deleted from the epithelium of the small intestine.

Materials and Methods

See the Supplementary Materials and Methods section for details.

Mice

The generation of *cytochrome P450-1a1Cre* (*Cyp1a1Cre*)[9] and *Ihh*$^{fl/fl}$[10] mice has been described previously. At 4 weeks of age, *Cyp1a1Cre-Ihh*$^{fl/fl}$ mice received intraperitoneal injections with either 80 mg/kg β-naphthoflavone (Sigma, St. Louis, MO) or vehicle (corn oil) for 5 days in a row. Mice were injected with 100 mg/kg bromodeoxyuridine (BrdU) (Sigma) intraperitoneally 1 hour before death and examined at 2 weeks, and at 1, 2, 4, and 6 months after recombination. Vehicle-injected *Cyp1a1Cre-Ihh*$^{fl/fl}$ and β-naphthoflavone–injected *Cyp1a1Cre-Ihh*$^{wt/wt}$ mice served as controls. For examination of recombination efficiency by Cre upon injections with β-naphthoflavone *Cyp1a1Cre* mice were crossed with *Rosa26Stop*$^{fl/fl}$*LacZ*[11] mice. The experiments were approved by the Institutional Animal Care and Use Committee of the University of Leiden and Amsterdam.

Immunohistochemistry, LacZ Staining, and In Situ Hybridization

Immunohistochemistry, LacZ staining, generation of probes, and in situ hybridization were performed using standard protocols. See the Supplementary Materials and Methods for more detail.

RNA Isolation, Complementary DNA Synthesis, and Quantitative Reverse-Transcription Polymerase Chain Reaction

For isolation of RNA from the duodenum a small piece of proximal tissue was collected. A detailed description of RNA isolation and complementary DNA (cDNA) synthesis can be found in the Supplementary Materials and Methods section. Quantitative reverse-transcription polymerase chain reaction (RT-PCR) was performed using Sybr Green (LightCycler 480 SYBR Green I Master, #04707516001; Roche, Basel, Switzerland) and pre-optimized primers from Qiagen (Hilden, Germany). *Glyceraldehyde-3-phosphate dehydrogenase* (*Gapdh*) was used as household gene. *Gapdh* expression was distributed equally between the wild-type and the *Ihh* mutant mice.

Statistics

Statistical analysis was performed with Prism 5.0 (GraphPad Software, La Jolla, CA). All values were represented as the mean ± standard error of the mean. Samples were analyzed using the Student *t* test. For multiple comparisons, a one-way analysis of variance was used followed by a Tukey post hoc test. Differences were considered statistically significant at a *P* value of less than .05.

Results

Loss of Ihh Signaling in Adult β-Naphthoflavone–Injected Cyp1a1Cre-Ihh$^{fl/fl}$ *Mice*

We examined expression of Ihh messenger RNA (mRNA) (Figure 1*A*) and protein (Figure 1*B*) in the small intestine of the mouse. Both Ihh protein and mRNA were expressed exclusively by the differentiated epithelial cells on the villi. To examine the role of Ihh signaling in the adult small intestinal mucosa we injected adult *Cyp1a1-Ihh*$^{fl/fl}$ mice and *Ihh*$^{fl/fl}$ control mice with β-naphthoflavone. This resulted in substantially reduced expression of Ihh protein (Figure1*B*, right panel). Quantitative RT-PCR showed sustained loss of *Ihh* expression at different time points after recombination (Figure 1*C*, $P < .001$ for all groups, $n \geq 4$/group). Loss of *Ihh* expression correlated with almost complete loss of Hh targets *Gli1* (86% re-

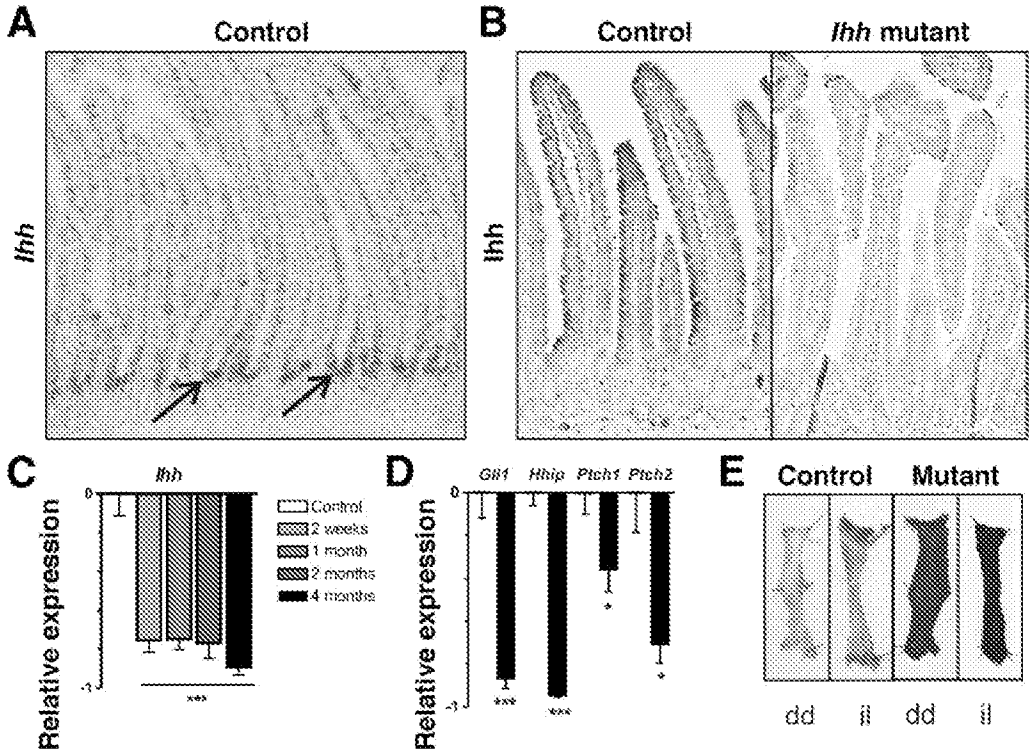

Figure 1. Loss of Ihh signaling from the small intestine in β-naphthoflavone–injected *Cyp1a1-Cre-Ihh*$^{fl/fl}$ adult mice. (*A*) In situ hybridization showed that *Ihh* mRNA was expressed exclusively by the epithelial cells on the villi. Expression was highest at the crypt villus junction (*arrows*) and diminished toward the villus tip. (*B*) Immunohistochemistry for Ihh showed expression of Ihh protein by the enterocytes on the villi in mice injected with solvent whereas β-naphthoflavone–injected mice have lost Ihh expression at 2 weeks after treatment (*right panel*). (*C*) Quantitative RT-PCR for *Ihh* at different time points and (*D*) Hh signaling targets *Gli1*, *Hhip*, *Ptch1*, and *Ptch2* two weeks after recombination (*black bars*) on intestinal homogenates of β-naphthoflavone–injected *Ihh*$^{fl/fl}$ control and *Cyp1a1-Cre-Ihh*$^{fl/fl}$ mice confirmed loss of *Ihh* expression. Original magnifications, 100×. (*C*) ****P* < .001. (*D*) **P* < .03; ****P* < .0001. (*E*) X-gal staining of the duodenum (dd) and ileum (il) of *Cyp1A1-stop*$^{fl/fl}$*LacZ* mice injected with vehicle (control) and β-naphthoflavone (mutant).

duced, $P < .0001$) and *Hhip* (94% reduced, $P < .0001$) but more modest reduction in *Ptch1* expression (36% reduced, $P = .03$) and *Ptch2* (65% reduced, $P = .03$) 2 weeks after recombination (n = 8 controls vs 6 *Ihh* mutants). Thus, expression of *Ptch1* and *Ptch2* may depend only partially on Hh signaling. X-gal staining of the small intestines of *Cyp1A1Cre-Rosa26Stop*$^{fl/fl}$*LacZ* mice showed efficient recombination along the proximo-distal axis of the small intestine (Figure 1*E*) as previously described.[9]

Loss of Ihh Is Sufficient to Initiate an Epithelial Wound Healing Response

Intestinal epithelial wound healing is characterized by increased epithelial proliferation and lengthening of crypts, which multiply by a process of budding and elongation termed *crypt fissioning* to replace lost crypts. We observed a strong increase in the rate of crypt fissioning in the *Ihh* mutant mice 2 weeks after recombination (Figure 2*A* and *B*, 3.3% in control mice vs 13.7% in mutant mice; $P < .001$, n = 5 per group). Two weeks later, when the crypts reached substantially increased density (1.7 and 3.0 crypts per 100 μm in the control [n = 8] vs *Ihh* mutant mice [n = 7]; $P < .001$, Figure 2*C*), the rate of crypt fissioning returned to normal (3.3%, n = 8, Figure 2*B*). Crypt fissioning returned again at 2 and 4 months in the context of chronic inflammation (see later). Crypts became progressively longer (from 66 μm in the controls to 154 μm in the *Ihh* mutant mice at 4 months [n > 4/time point]; $P < .001$ for control vs 4 mo) and a transient modest increase in villus length was observed (Supplementary Figure 1). Changes were measured in the duodenum but were similar in the rest of the small intestine (data not shown). *Ihh* mutant mice showed an increase in BrdU-positive cells (Figure 2*E* and *F*) with 6.9 BrdU-positive cells per crypt in controls (n = 5), 11.7 at 2 weeks (n = 5, $P < .01$), and 14.2 at 1 month (n = 7, $P < .001$). Although the total number of BrdU-positive cells per crypt increased, the relative number of positive cells per crypt cell (labeling index) remained stable. Because we previously found an inhibitory role of Hh signaling on Wnt signaling[1,3] we investigated the effect of loss of Ihh on Wnt signaling 1 months after recombination. The hallmark of activated Wnt signaling in intestinal epithelial cells is nuclear accumulation of β-catenin,[12] which was increased in mutant mice compared with controls (Figure 3*A* and *B*; 1.9 positive nuclei in *Ihh* mutants [n = 6] vs 1.1 per crypt in controls; n =

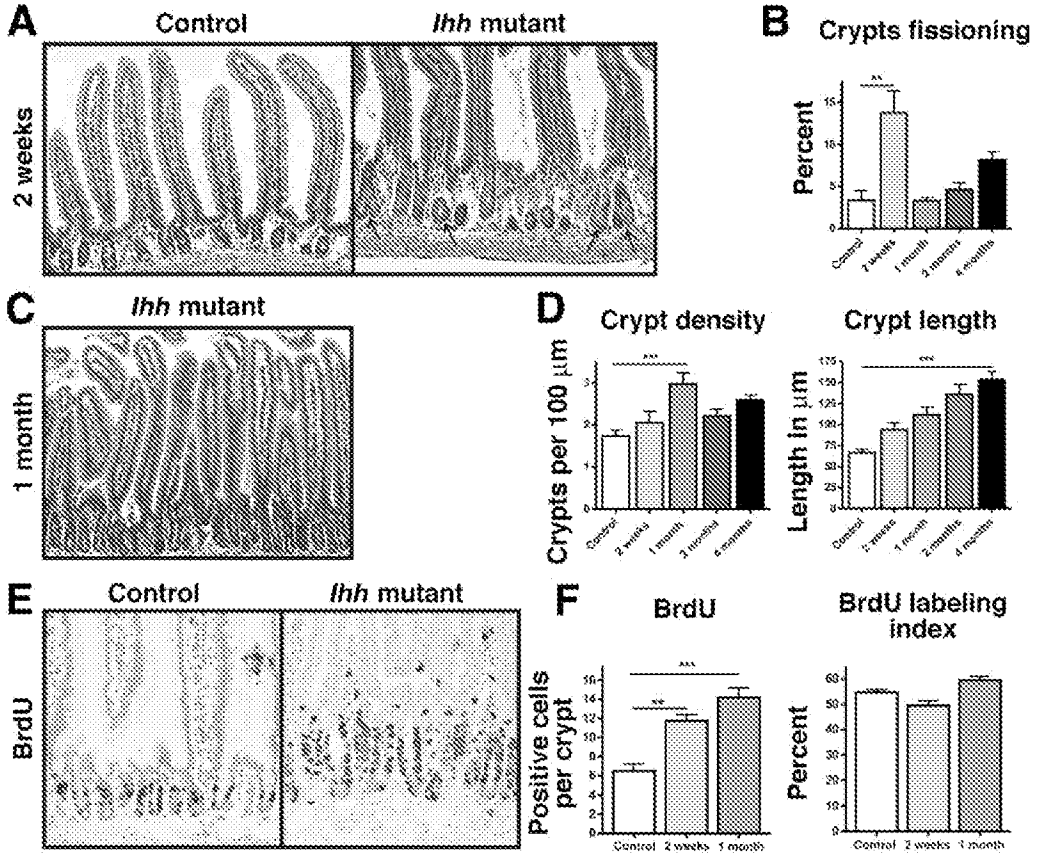

Figure 2. Loss of Ihh is sufficient to initiate a regenerative response. (*A* and *B*) A strong increase in the rate of crypt fissioning was observed (*A*, *arrows* show fissioning crypts), (*B*) which was maximal 2 weeks after recombination. $^{**}P < .001$. (*C*) H&E staining of the duodenum showed increased crypt density, deepening of crypts, and lengthening of the villi in the *Ihh* mutant mice 1 month after injection with β-naphthoflavone. (*D*) Measurements of crypt density and crypt length confirmed an increase in the *Ihh* mutant mice 1 month and 4 months after recombination, respectively. $^{***}P < .001$. (*E*) Immunohistochemistry for BrdU at 1 month after recombination. (*F*) BrdU-positive cells were counted and set out both as absolute number of positive cells per crypt and as labeling index, an indication for the percentage of cells per crypt that were positive for BrdU. $^{**}P < .01$; $^{***}P < .001$ Original magnifications, (*A*, *left panel*, and *C*) 100×, and (*A*, *right panel*, and *E*) 200×.

4; $P = .01$). We examined the expression of targets of Wnt signaling, EphB2 and EphB3, and Cd44[13] by immunohistochemistry and stem cell markers *Lgr5* and *Olfm4* by in situ hybridization. All were increased in the *Ihh* mutant mice (Figure 3*C* and *D* and Supplementary Figure 2). We examined the 4 different epithelial cell lineages in the small intestine 1 month after recombination (Figure 3*E* and *F* and Supplementary Figure 3). We observed a modest increase in the numbers of Paneth cells at the base of the crypts (Supplementary Figure 3*A*), which was stable in time. Electron microscopy showed incomplete microvillus formation on the enterocytes 1 month after recombination (Figure 3*E*), confirming our previous finding that Hh signaling is required for proper enterocyte differentiation.[1] A histochemical staining for alkaline phosphatase activity, a marker of differentiated epithelial cells, showed that the layer containing alkaline phosphatase became slightly thinner over time and disappeared completely 4 months after recombination (Figure 3*F*).

Loss of Epithelial Smad Signaling in Ihh Mutant Mice

We examined Bmp signaling by immunohistochemistry using a phospho-specific antibody against the Bmp signaling specific, phosphorylated Smads 1, 5, and 8 (pSmad1,5,8), by quantitative RT-PCR for *Bmp2, 4*, and *7* and of Bmp targets *Id1-4*. Nuclear pSmad1,5,8 staining was observed in the villi of control mice whereas the crypts were negative as described.[7] Loss of *Ihh* expression lead to almost complete loss of pSmad1,5,8 (Figure 4*A*), which correlated with loss of *Bmp4* expression (Figure 4*B*; $P < .0001$; n = 7/group) and reduced expression of *Id1* and *3* (Figure 4*C*; $P = .04$ and $P = .004$, respectively; n = 7/group). Because pSmad1,5,8 signaling was restricted to differentiated cells, loss of Bmp signaling is no explanation for increased proliferation in the crypts of mutant mice. We therefore examined the localization of phosphorylated Smads 2 and 3 (pSmad2,3; Figure 4*D*), which mediate Tgfβ/Activin signaling. Intriguingly, we found that activity of Smad1,5,8 and Smad2,3 is mutually ex-

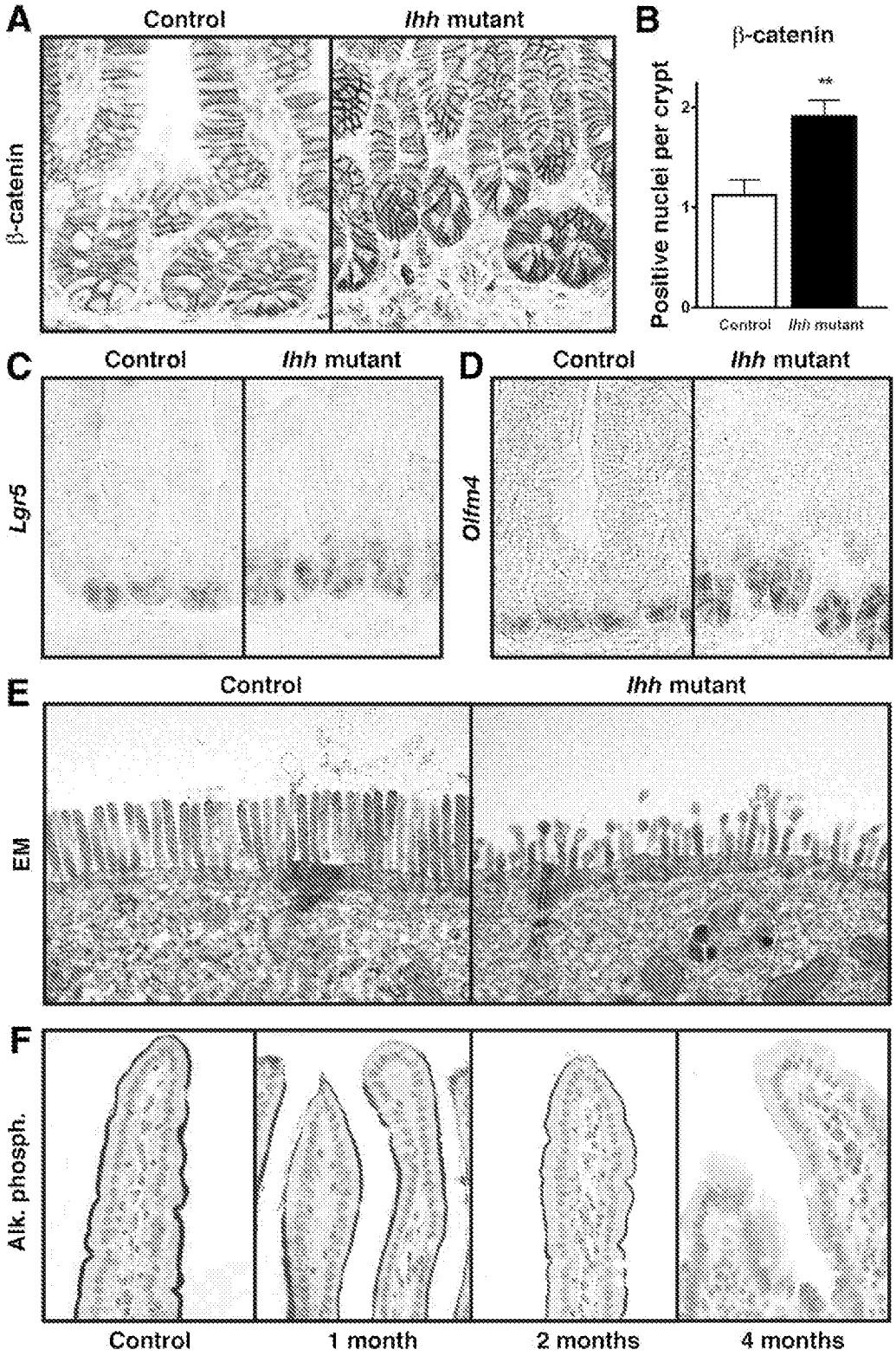

Figure 3. Increased Wnt signaling upon loss of Ihh. (*A*) Immunohistochemistry for β-catenin. (*B*) An increase in the number of positive nuclei per crypt was observed in the *Ihh* mutant mice. $^{**}P < .01$. In situ hybridization for (*C*) *Lgr5* and (*D*) *Olfm4* showed an increase in cells positive for these stem cell markers 1 month after recombination. (*E*) Incomplete formation of microvilli in the mutant mice 1 month after recombination. (*F*) Alkaline phosphatase was still present 2 months after recombination but had disappeared from the remaining villi 4 months after recombination. Original magnifications, 400×.

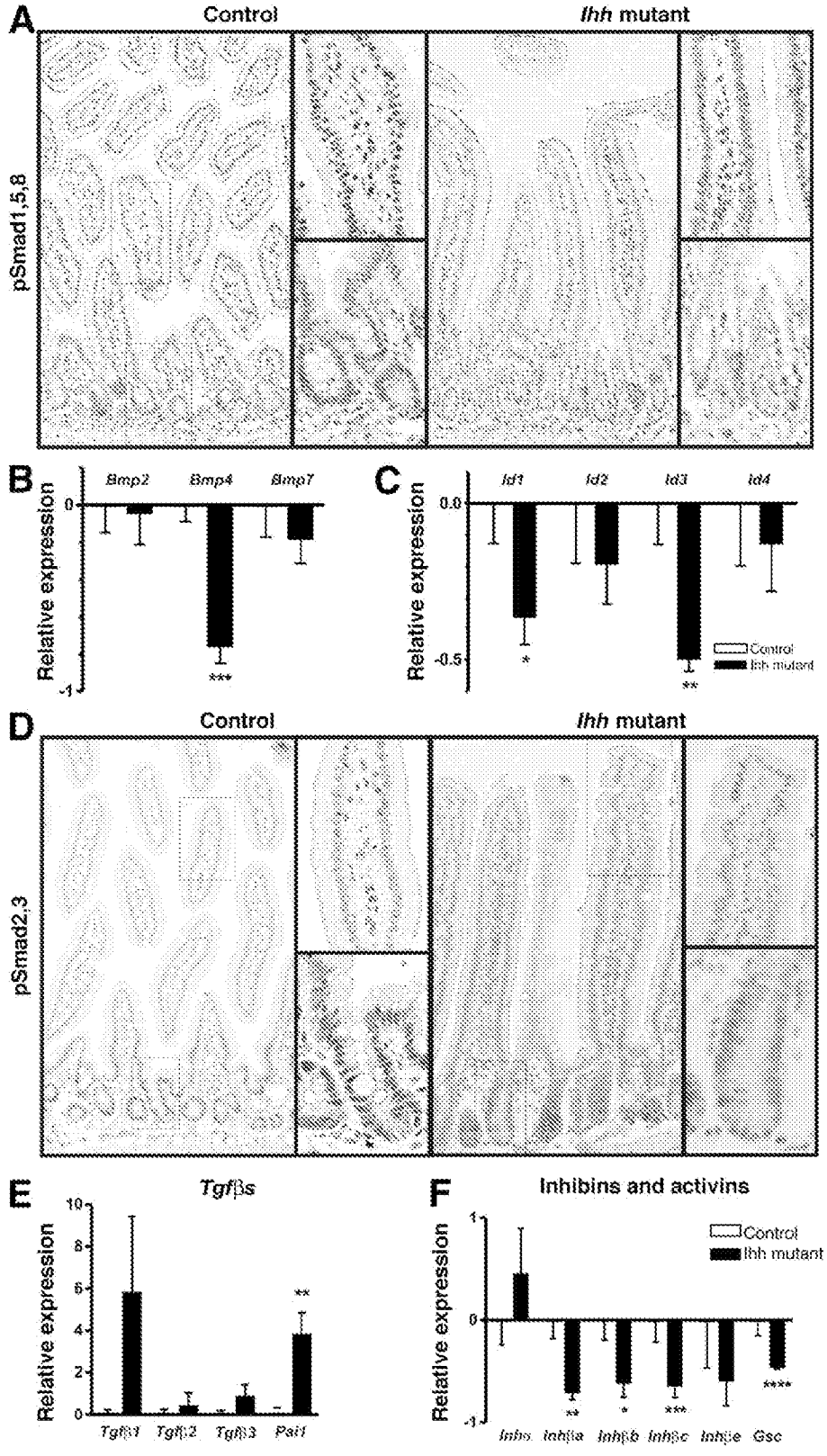

Figure 4. Loss of Ihh signaling leads to reduced Bmp and Activin signaling in the epithelium of *Ihh* mutant mice and increases Tgfβ signaling. (*A*) Immunohistochemistry for Bmp-associated pSmad1,5,8 showed nuclear staining in the villi of control mice, whereas the crypts were negative. One month after recombination the staining was reduced in *Ihh* mutants. (*B*) Quantitative RT-PCR for *Bmp2*, *Bmp4*, *Bmp7*, and (*C*) targets *Id1-4*, showed a significant reduction in the expression of *Bmp4*, which correlated with reduced *Id1* and *Id3*. $^{*}P < .04$; $^{**}P < .004$; $^{***}P < .0001$. (*D*) Immunohistochemistry for Tgfβ/Activin-associated pSmad2,3 showed exclusive signaling by Smad2 and 3 in the epithelial cells of the crypts. Upon loss of Hh signaling the staining in the crypts was lost. (*E*) Quantitative RT-PCR showed a nonsignificant up-regulation of the *Tgfβs*, mainly of *Tgfβ1*, and a significant up-regulation of *Pai-1*, a target of Tgfβ signaling. $^{**}P < .005$. (*F*) Quantitative RT-PCR for the different *Inhibins* showed that *Inhibinα*, which is needed to form Inhibins, was up-regulated, and that the different *Inhibinβs* (*βa*, *βb*, *βc*, and *βe*, which are subunits needed to form the Activins) were down-regulated. $^{*}P < .022$; $^{**}P < .003$; $^{***}P < .02$; $^{****}P < .01$. Original magnifications: (*A* and *D*, *large panels*) 100× and (*A* and *D*, *enlargements*) 400×.

clusive because the expression of pSmad2,3 was restricted to the epithelial cells in the crypt (Figure 4*D*). One month after recombination, pSmad2,3 in the crypts was strongly reduced (Figure 4*D*). However, quantitative RT-PCR for *Tgfβs* and signaling target *Plasminogen activator inhibitor-1* (*Pai-1*) (Figure 4*E*) showed an increase in *Tgfβ* expression, although not significantly ($P = .17$ for *Tgfβ1*; $P = .63$ for *Tgfβ2*; and $P = .27$ for *Tgfβ3*; n = 7/group). *Pai-1* expres-

sion was increased significantly ($P = .005$; n = 7/group). Immunohistochemistry for Pai-1 showed that up-regulation occurred mainly in the villus mesenchyme (Supplementary Figure 4), whereas no epithelial staining was observed. The lack of correlation between pSmad2, 3 expression and *Tgfβ* signaling suggested that pSmad2, 3 in the crypts may depend on Activin signaling. Activins are dimeric proteins and are composed of 2 Inhibinβ subunits, whereas Inhibins, antagonists of Activins, are composed of an Inhibinα and an Inhibinβ subunit. We examined the expression of different *Inhibins* and of *Goosecoid*, a conserved target of Activin signaling[14] (Figure 4*F*). Two *Goosecoid* genes are present in mouse and human beings (*Goosecoid* and *Goosecoid2*). We found a nonsignificant up-regulation of the Inhibin-specific *Inhibinα* ($P = .4$) and a down-regulation of all *Inhibinβs* ($P = .003$ for *Inhibinβa*; $P = .022$ for *Inhibinβb*; $P = .02$ for *Inhibinβc*; and $P = .31$ for *Inhibinβe*; n = 7/group). Expression of *Inhibinβe* was very low in both control and mutant mice. Expression of Activin target *Goosecoid* was reduced ($P = .01$; n = 7 for both groups), expression of *Goosecoid2* was undetectable. Thus, our data suggest that Ihh is required to maintain Bmp signaling in the differentiated epithelial cells on the villus and Activin signaling in the crypts.

Loss of Ihh Resulted in Influx of Macrophages and Fibroblasts Into the Villus Core

Because we observed an increased cellularity of the lamina propria of the villi after recombination (Figure 5*A*) we carefully examined the mesenchyme for inflammatory cells, markers of (myo)fibroblasts, and smooth muscle cells. We observed a dramatic increase in the number of F4/80-positive macrophages in the villus core from 2 weeks after recombination, which was stable in time (Figure 5*B*; 17 macrophages per villus in the control mice vs 39 in the mutant mice at 2 weeks; n = 3 and n = 4 respectively; $P < .01$). Macrophages in the crypt area appeared at later stages (see later). In addition to the macrophages we observed a strong increase in the number of vimentin-positive cells, mainly around the crypt villus junction at 2 weeks but throughout the crypt villus mesenchyme at 1 month (Figure 5*C*; from 10.7 positive cells in the controls [n = 5] to 19.7 positive cells at 2 weeks [n = 4; $P < .05$] and 39 positive cells at 1 month [n = 4; $P < .01$]) We examined whether these vimentin-positive cells could be fibroblasts by staining for S1004A (Fibroblast-specific protein-1). The number of S100A4-positive cells was increased from the 2-week time point (Figure 5*D*; 0.8 S100A4-positive cells per villus in the control mice vs 10.2 in the mutant mice at 2 weeks; $P < .001$). To further examine the nature of the vimentin-positive cells we performed double stainings for vimentin and macrophage marker Cd68 and for vimentin and S1004A. The vimentin-positive cells were negative for Cd68 (Figure 5*E*), but positive for fibroblast marker S1004A (Figure 5*F*), indicating that most vimentin-positive cells were fibroblasts. Thus, loss of Ihh not only results in epithelial changes that are highly similar to a wound healing response but also to the recruitment of 2 of the principal cell types that play a role in wound healing, macrophages and fibroblasts.

Loss of Smooth Muscle Cells in Ihh Mutant Mice

Analysis of the expression of α-smooth muscle actin (α-Sma) and desmin in the normal mouse showed mainly desmin single-positive cells (smooth muscle cells) and desmin–α-Sma double-positive cells (smooth muscle precursor cells) (Supplementary Figure 5). We observed only rare α-Sma single-positive cells in the villus cores because under normal circumstances myofibroblasts are located mainly in the pericrypt areas.[15] Their number is increased during wound healing, in inflamed tissues, and in tumor stroma.[15,16] *Ihh* mutant mice showed a sequential and almost complete loss of the expression of α-Sma and desmin (Supplementary Figure 6*A* and *B*). First, α-Sma expression was lost around the 1-month time point with only rare remaining cells in the villus core. Desmin expression was lost between 2 and 4 months after recombination. We observed a substantial morphologic change in the α-Sma–positive and desmin-positive cells before they lost expression of these markers. These cells normally have an elongated appearance but rolled up into rounded cells after loss of *Ihh* at the earliest time point examined (Supplementary Figure 6*C* and *D*). No apoptosis of mesenchymal cells was observed at any time point (2 weeks, and at 1, 2, and 4 months) after recombination using an active caspase-3 antibody and an appropriate positive control (data not shown), suggesting that smooth muscle cells are not lost by apoptosis.

Prolonged Loss of Ihh Results in Progressive Leukocyte Infiltration of the Crypt Area, Villous Atrophy, and the Development of Intestinal Fibrosis

At 4 months after recombination *Ihh* mutant mice developed chronic enteritis (Figure 6*A* and *B*). The inflammation was characterized by a mixed infiltrate, consisting of macrophages, neutrophils, and T cells, and the presence of edema and blunting of small intestinal villi (Figure 7*A*). Macrophages increased from 1.3 F4/80-positive cells per intercrypt area in the control mice (n = 3) to 16.3 positive cells 4 months after recombination (n = 4; $P < .001$). Neutrophils increased from 0 Ly6G-positive cells per intercrypt area in control mice (n = 5) to 8.8 positive cells 4 months after recombination (n = 5; $P < .001$). T cells changed from 0 Cd3-positive cells per intercrypt area in the control mice (n = 8) to 6.3 positive cells 4 months after recombination (n = 4; $P < .001$). Because profound changes in the composition and morphology of cells in the lamina propria preceded the development of inflammation, we examined the epithelial

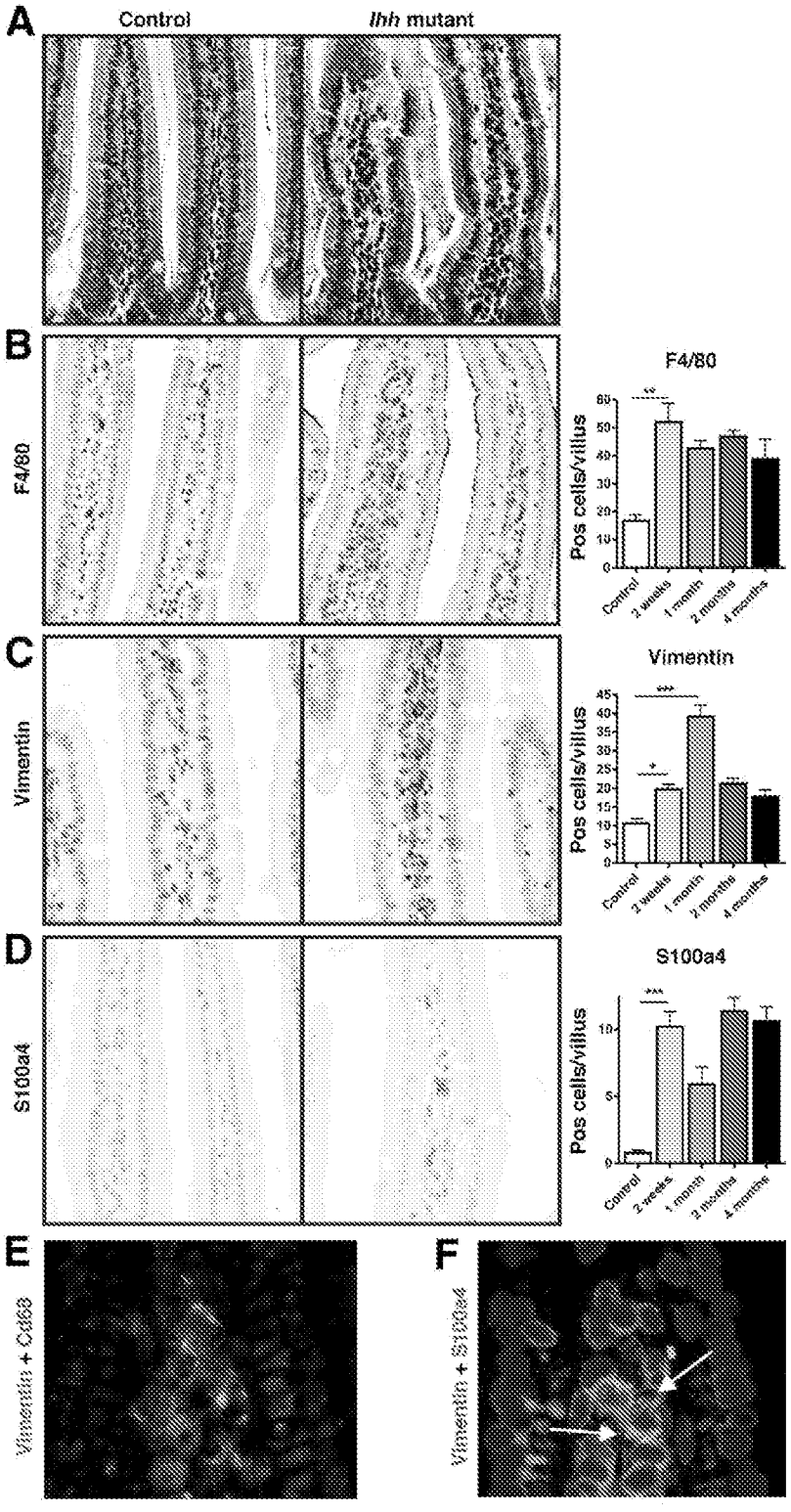

Figure 5. Influx of macrophages and fibroblasts into the villus core. (*A*) H&E stainings showed increased cellularity of the villus core 1 month after recombination compared with the control group. An influx of (*B*) macrophages (F4/80-positive cells), (*C*) vimentin-positive cells, and (*D*) fibroblasts (S1004A-positive cells) was observed at this time point. (*B–D*) Counting of macrophages, vimentin-positive cells, and fibroblasts showed recruitment from the earliest time point examined (*graph*). (*B*) $^{**}P < .01$. (*C*) $^{*}P < .05$; $^{***}P < .01$. (*D*) $^{***}P < .001$. (*E*) A double staining for vimentin (*green*) and Cd68 (*red*) showed no double staining 1 month after recombination. (*F*) A double staining for vimentin (*red*) and S1004A (*green*) showed that part of the vimentin-positive cells also were S1004A-positive (*white arrows*). Original magnifications, 400×.

barrier function of the *Ihh* mutant mice at 1 month after recombination (before the first overt epithelial damage) using different techniques but found no defect in epithelial barrier function (Supplementary Figure 7). Blunting of the villi was increasingly pronounced along the proximal-distal axis of the small intestine (Figure 6*A* and *B*), giving large parts of the small intestine the appearance of colonic mucosa. In contrast to the development of an inflammatory infiltrate in the crypt area (Figure 7*A*) we observed almost complete loss of Cd3-positive intraepithelial lymphocytes at 4 months and substantial loss of T cells from the villus core (Supplementary Figure 8). At 6

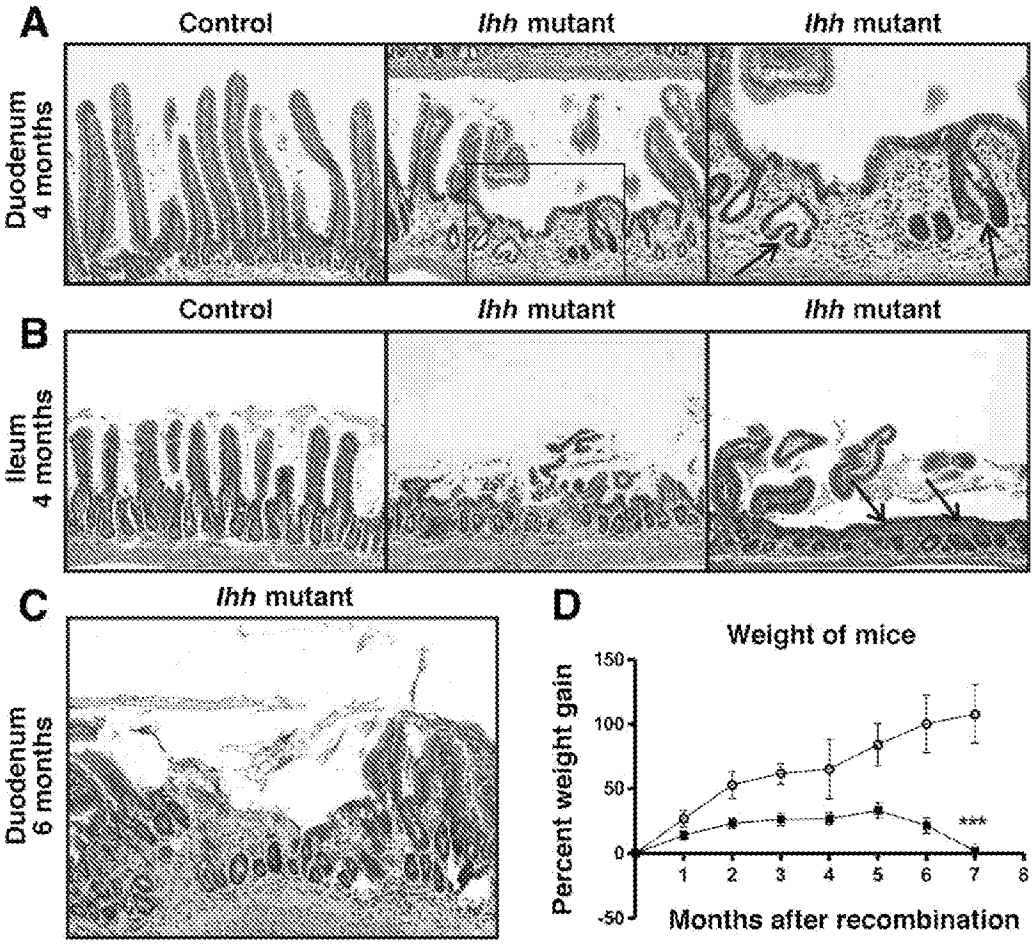

Figure 6. Loss of Ihh resulted in the development of chronic enteritis with villous atrophy. (*A*) Compared with control duodenum the duodenum of *Ihh* mutant mice showed the development of a chronic inflammatory infiltrate with partial loss of villi. Crypts displayed increased depth and fissioning (*arrows*), as also was observed at earlier time points. (*B*) In the ileum, epithelial damage was more severe and loss of villi was almost complete. In some parts of the ileum the epithelium had entirely covered the damaged mucosal layer (*arrows*), giving the crypts a buried appearance. (*C*) At 6 months after recombination at some places erosion had developed. (*D*) The *Ihh* mutant mice, which where behind in weight gain from the moment of recombination, started losing weight at 5 months of recombination. ***$P < .001$. Original magnifications, (*A*–*C*, *left panels*) 100×, and (*A*, *enlargement*) 200×.

months after recombination the villous atrophy and inflammation was progressively worse. The structure of the few remaining villus cores was gone, and in most of the small intestine the villi were now completely gone. At some places erosions were observed (Figure 6*E*). The *Ihh* mutant animals had not been growing as well as the control mice since the moment of recombination, and at 5 months after recombination they started losing weight, whereas the control mice kept gaining weight (Figure 6*F*). They weighed significantly less than the control group ($P < .001$). Even though mutant mice were losing weight at this stage no blood loss or diarrhea was observed and their stools had a normal appearance.

Because the epithelial remodeling and influx of fibroblasts and macrophages are characteristic of a wound healing response we examined the mucosa for possible changes in the extracellular matrix. A Sirius red stain for collagen showed progressive accumulation of collagen in the lamina propria from 2 weeks after recombination onward, ultimately resulting in an extensive accumulation in between the crypts (Figure 7*B*). The presence of intestinal fibrosis was further confirmed by immunohistochemistry for fibronectin, which showed a similar progressive accumulation in the lamina propria (Figure 7*C*). Thus, loss of Ihh results in the progressive development of intestinal fibrosis.

Discussion

We find that loss of Ihh results in an epithelial response that is characteristic of epithelial wound repair and is associated with loss of both Bmp and Activin signaling in the epithelial cells. In addition to the epithelial remodeling we observed substantial recruitment of macrophages and fibroblasts, 2 critical mesenchymal cell types involved in wound repair, into the villus core. Unresolved loss of Ihh ultimately results in loss of smooth muscle cells, the establishment of a pericryptal mixed inflammatory infiltrate, loss of villi, mucosal erosions, and the development of extensive intestinal fibrosis.

The most salient feature of a wound repair response in the *Ihh* mutant mice is the rapid increase in the rate of epithelial proliferation, crypt fissioning, and lengthening of crypts. Although the increase in crypt length is progressive in time, the rate of crypt fissioning returns to control levels at 1 month after recombination when crypt density is increased markedly. This suggests that at this increased density an Ihh-independent mechanism is ac-

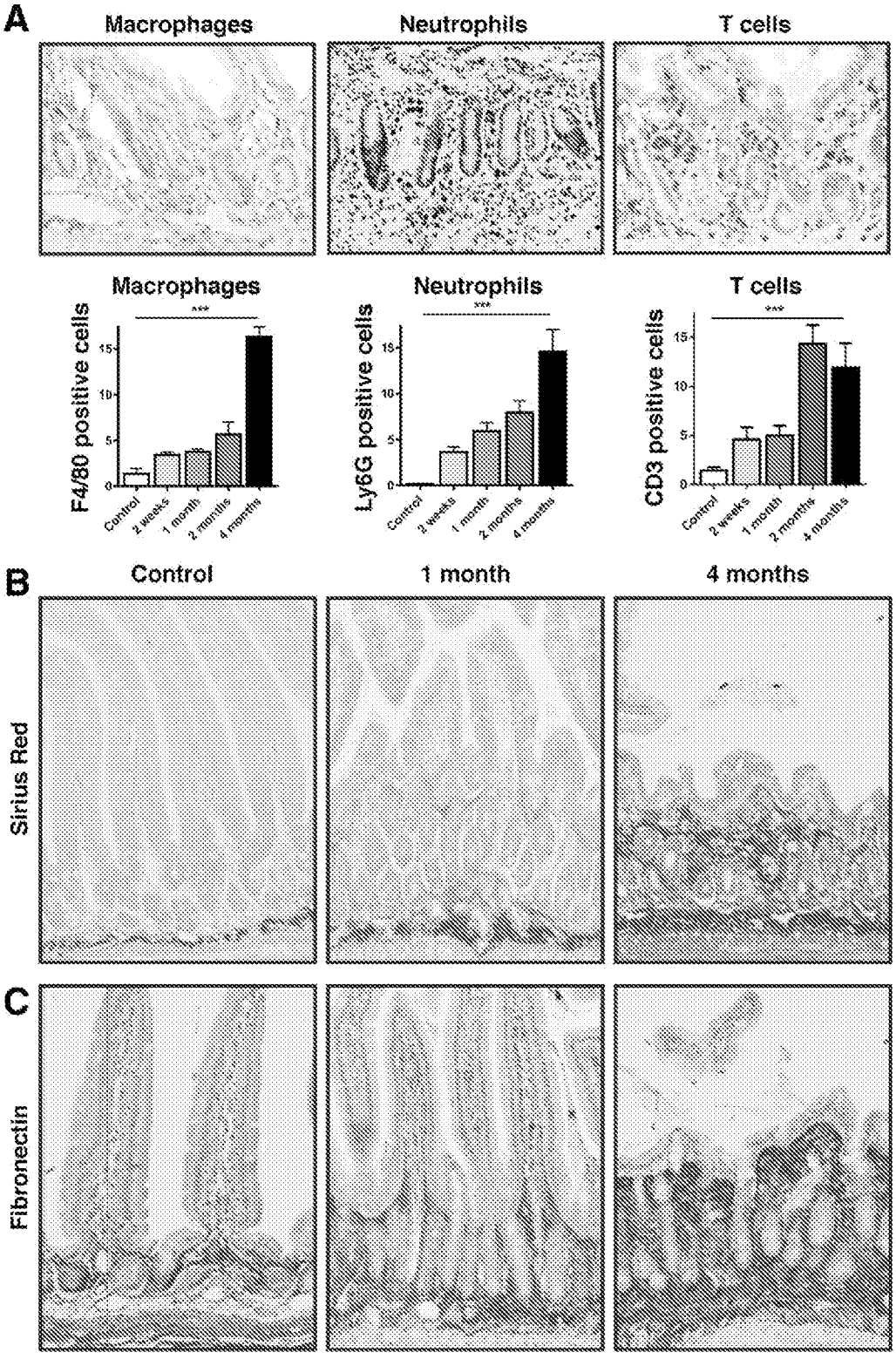

Figure 7. Infiltration of inflammatory cells and development of intestinal fibrosis in the *Ihh* mutant mice. (*A*) Four months after recombination an inflammatory infiltrate appeared in the crypt area of the *Ihh* mutant mice, consisting of macrophages (F4/80-positive), neutrophils (Ly6G-positive), and T cells (Cd3 positive). ***$P < .001$. Progressive accumulation was observed of (*B*) collagen and (*C*) fibronectin in the lamina propria. Original magnifications, (*A*) 400× and (*B* and *C*) 200×.

tivated that stops crypt fissioning. The epithelial changes observed in the *Ihh* mutant mouse are very similar to the adaptive response that is observed after massive small-bowel resection.[17,18] It previously was found by others that expression of *Ihh* and Hh target genes are almost completely lost after massive small-bowel resection in the mouse.[19] Our data now show that this is in fact sufficient to initiate the adaptive response in the absence of loss of intestinal tissue or intestinal damage.

The epithelial remodeling events were associated with an almost complete loss of Smad signaling from the epithelium. Loss of phosphorylation of the Bmp-specific

Smads1, 5, and 8 was associated with loss of *Bmp4* expression, which previously has been shown to be expressed in the small intestinal mesenchyme.[6,7] However, because pSmad1,5,8 is not normally observed in the crypt epithelial cells its loss cannot be directly responsible for the crypt budding and elongation phenotype in *Ihh* mutant mice. This suggests a role for one or more additional signaling pathways, acting directly on the epithelial cells of the crypt. We found that the key mediators of Tgfβ and Activin signaling pSmad2 and 3 were active in normal crypts. The activity of Smads1,5,8 and Smads2,3 is therefore mutually exclusive. Interestingly, it previously has been found that Smad1 can compete with Smads 2 and 3 for Smad4, the common mediator required for all Smad signaling to establish a bistable system (left vs right) in the establishment of left–right asymmetry in the early embryo.[20] It will be intriguing to examine the role of the nonoverlapping pattern of Smad activity along the crypt-villus axis. In the *Ihh* mutant mouse, pSmad2,3 was lost from the crypt and this loss may be one of the factors that result in the increased crypt fissioning, Wnt signaling, and epithelial proliferation. Because Tgfβ signaling was up-regulated and Tgfβ target Pai-1 localized exclusively to the villus mesenchyme, loss of pSmad2,3 from the crypt is unlikely to be related to changes in Tgfβ signaling. Loss of pSmad2,3 was associated with a down-regulation of Inhibinβs, which encode for the subunits that form the Activins. Thus, our results suggest that Activins may be one of the mesenchymal signals that control crypt cell fate in response to Ihh derived from the differentiated cells.

The second important feature that is reminiscent of a wound healing response in the *Ihh* mutant mice is the substantial recruitment of both macrophages and fibroblasts to the lamina propria. Macrophages are a key component of the inflammatory phase of the wound healing response.[21] A third feature of the *Ihh* mutant mouse that resembles wound healing is the deposition of extracellular matrix proteins in the lamina propria. We observed a progressive accumulation of both collagen and fibronectin from week 2 onward. The fourth feature that is reminiscent of wound healing in the *Ihh* mutants is the apparent increase in Tgf-β signaling with appearance of Pai-1–positive cells in the mesenchyme.

Thus, loss of *Ihh* results in several aspects of a wound healing response such as epithelial remodeling, recruitment of macrophages and fibroblasts, and the deposition of extracellular matrix proteins. This suggests that the loss of Ihh protein expression that would be associated with loss of superficial intestinal epithelial cells is in itself sufficient to cause several key aspects of wound healing. In a normal wound the wound bed would soon be covered with fresh epithelial cells, thus slowly restoring Ihh signaling to the underlying lamina propria cells. The later time points examined in the *Ihh* mutant mice may therefore represent an unresolved wound healing response. Indeed, prolonged loss of Ihh results in the progressive accumulation of inflammatory cells around the crypts, and the development of mucosal damage and extensive intestinal fibrosis. This is an intriguing finding in light of the recent association between hypomorphic single nucleotide polymorphisms in the Hh transcription factor *GLI1* and the development of inflammatory bowel disease.[8]

Because the loss of villi seems to occur concurrent with the complete loss of α-Sma and desmin-positive cells it may be that the villi disintegrate owing to the loss of these villus core cells that may act to anchor the villi into the intestinal mucosa. The villus atrophy shows an intriguing resemblance to the histology observed in patients with celiac disease. Even the ultrastructural changes of the microvilli on the enterocytes are typical for those observed in celiac disease.[22] However, we find that there is loss of intraepithelial lymphocytes in the *Ihh* mutant mice rather than the accumulation that is one of the hallmarks of celiac disease. It is unlikely that loss of Ihh signaling plays a causal role in the development of celiac disease. It may be, however, that loss of epithelial Ihh expression results from the immunologic response to gluten in patients with celiac disease and therefore does contribute to the development of villus atrophy.

Because the smooth muscle cells are at least numerically the most important Hh target cells in the intestinal mucosa loss of Hh signaling in these cells may result in the coordination of the multiple changes observed in the *Ihh* mutant mice. Experiments currently are underway in our laboratory to examine more precisely the molecular changes in the Hh target cells that seem to result in the activation of a wound healing–like mucosal response.

As we prepared a revised version of this article a study with many similarities to our observations was published.[6] In this study by Zacharias et al, Hh antagonist Hhip specifically was expressed in the intestinal epithelium from around birth. Thus, in this model Hhip is expressed during postnatal development of the intestine during which the intestine undergoes rapid growth and the crypt–-villus system is established. Zacharias et al observe a similar proliferative response of the epithelium and loss of smooth muscle cells and a similar histology that is reminiscent of celiac disease at later stages. Our data show that the phenotype is not related to disruption of Hh during postnatal development of the intestine, at which time the crypts are being formed and the villus core is still developing, but is similar when Hh signaling is lost in a fully developed adult intestine.

In conclusion, we find that Ihh not only acts as a negative feedback regulator of the epithelial cells but that loss of expression is sufficient to cause several aspects of an intestinal wound healing response. Unresolved loss of Ihh is ultimately detrimental to the intestine with the development of chronic enteritis, mucosal damage, and intestinal fibrosis. Our data suggest that the Ihh signal

derived from the superficial epithelium may act as a critical sensor of epithelial integrity in the intestine.

Supplementary Material

Note: To access the supplementary material accompanying this article, visit the online version of *Gastroenterology* at www.gastrojournal.org, and at doi: 10.1053/j.gastro.2010.07.045.

References

1. van den Brink GR, Bleuming SA, Hardwick JC, et al. Indian Hedgehog is an antagonist of Wnt signaling in colonic epithelial cell differentiation. Nat Genet 2004;36:277–282.
2. Madison BB, Braunstein K, Kuizon E, et al. Epithelial hedgehog signals pattern the intestinal crypt-villus axis. Development 2005;132:279–289.
3. van Dop WA, Uhmann A, Wijgerde M, et al. Depletion of the colonic epithelial precursor cell compartment upon conditional activation of the hedgehog pathway. Gastroenterology 2009; 136:2195–2203.
4. Kolterud A, Grosse AS, Zacharias WJ, et al. Paracrine hedgehog signaling in stomach and intestine: new roles for hedgehog in gastrointestinal patterning. Gastroenterology 2009;137:618–628.
5. Roberts DJ, Johnson RL, Burke AC, et al. Sonic hedgehog is an endodermal signal inducing Bmp-4 and Hox genes during induction and regionalization of the chick hindgut. Development 1995; 121:3163–3174.
6. Zacharias WJ, Li X, Madison BB, et al. Hedgehog is an anti-inflammatory epithelial signal for the intestinal lamina propria. Gastroenterology 2010;138:2368–2377.
7. Haramis AP, Begthel H, van den BM, et al. De novo crypt formation and juvenile polyposis on BMP inhibition in mouse intestine. Science 2004;303:1684–1686.
8. Lees CW, Zacharias WJ, Tremelling M, et al. Analysis of germline GLI1 variation implicates hedgehog signalling in the regulation of intestinal inflammatory pathways. PLoS Med 2008;5:e239.
9. Ireland H, Kemp R, Houghton C, et al. Inducible Cre-mediated control of gene expression in the murine gastrointestinal tract: effect of loss of beta-catenin. Gastroenterology 2004;126:1236–1246.
10. Razzaque MS, Soegiarto DW, Chang D, et al. Conditional deletion of Indian hedgehog from collagen type 2alpha1-expressing cells results in abnormal endochondral bone formation. J Pathol 2005; 207:453–461.
11. Soriano P. Generalized lacZ expression with the ROSA26 Cre reporter strain. Nat Genet 1999;21:70–71.
12. van de Wetering M, Sancho E, Verweij C, et al. The beta-catenin/TCF-4 complex imposes a crypt progenitor phenotype on colorectal cancer cells. Cell 2002;111:241–250.
13. Batlle E, Henderson JT, Beghtel H, et al. Beta-catenin and TCF mediate cell positioning in the intestinal epithelium by controlling the expression of EphB/ephrinB. Cell 2002;111:251–263.
14. Cho KW, Blumberg B, Steinbeisser H, et al. Molecular nature of Spemann's organizer: the role of the Xenopus homeobox gene goosecoid. Cell 1991;67:1111–1120.
15. Powell DW, Mifflin RC, Valentich JD, et al. Myofibroblasts. I. Paracrine cells important in health and disease. Am J Physiol 1999;277:C1–C9.
16. Eyden B, Banerjee SS, Shenjere P, et al. The myofibroblast and its tumours. J Clin Pathol 2009;62:236–249.
17. Dowling RH, Booth CC. Functional compensation after small-bowel resection in man. Demonstration by direct measurement. Lancet 1966;2:146–147.
18. Dekaney CM, Fong JJ, Rigby RJ, et al. Expansion of intestinal stem cells associated with long-term adaptation following ileocecal resection in mice. Am J Physiol Gastrointest Liver Physiol 2007;293:G1013–G1022.
19. Tang Y, Swietlicki EA, Jiang S, et al. Increased apoptosis and accelerated epithelial migration following inhibition of hedgehog signaling in adaptive small bowel postresection. Am J Physiol Gastrointest Liver Physiol 2006;290:G1280–G1288.
20. Furtado MB, Solloway MJ, Jones VJ, et al. BMP/SMAD1 signaling sets a threshold for the left/right pathway in lateral plate mesoderm and limits availability of SMAD4. Genes Dev 2008;22: 3037–3049.
21. Martin P, Leibovich SJ. Inflammatory cells during wound repair: the good, the bad and the ugly. Trends Cell Biol 2005;15:599–607.
22. Shiner M. Ultrastructural changes suggestive of immune reactions in the jejunal mucosa of coeliac children following gluten challenge. Gut 1973;14:1–12.

Received August 27, 2009. Accepted July 19, 2010.

Reprint requests

Address requests for reprints to: Willemijn A. van Dop, MD, Center for Experimental Molecular Medicine, G2-105, Academic Medical Center, 1105 AZ Amsterdam, The Netherlands. e-mail: w.a.vandop@amc.uva.nl; fax: 31 20 6977192.

Conflicts of interest

The authors disclose no conflicts.

Funding

The research leading to these results has received funding from the European Research Council under the European Community's Seventh Framework Program (FP7/2007-2013)/European Research Council grant agreement number 241344 and by a grant from the Dutch Digestive Foundation. Generation of floxed Ihh mice was funded by the National Institutes of Health (AR050560 to B.L.).

Supplementary Materials and Methods

Histology and Morphometry

H&E staining was performed following standard procedures. For morphometry the software program ImageJ (freely available at: rsbweb.nih.gov/ij/) was used. Length of crypts and villi were measured in at least 15 crypts and villi per mouse were measured in at least 2 different regions of the duodenum. The percentage of fissioning crypts was counted per 250 crypts in each mouse. We defined a crypt as a fissioning crypt from the moment we could see the development of a fissure that bisected the crypt base creating 2 (or more) crypts to the moment that this fissure reached the lumen and the appearance of a bifurcating crypt had disappeared.

Immunohistochemistry

Slides were deparaffinized, dehydrated, and immersed in 1.5% H_2O_2 in phosphate-buffered saline (PBS) for 30 minutes. We used different methods of antigen retrieval.

NaCi. Slides were cooked at 100°C for 20 minutes in 0.01 mol/L sodium citrate (pH 6).

Tris/ethylenediaminetetraacetic acid. Slides were cooked at 100°C for 20 minutes in Tris/ethylenediaminetetraacetic acid (EDTA) buffer (10 mmol/L Tris, 1 mmol/L EDTA, pH 9).

HCl and pepsin. DNA was denaturated in 2 N HCl for 30 minutes at 37°C. Slides were prerinsed in 0.1 mol/L $Na_2B_4O_7$ (borax) 3 times for 5 minutes and subsequently thoroughly rinsed in PBS. Enzymatic pretreatment was performed by incubating slides in 0.4% (wt/vol) pepsin in 0.01 N HCL for 30 minutes at 37°C.

Proteinase K. Slides were incubated for 15 minutes at 37°C in proteinase K solution, 19 mL of TE buffer (6.1 g Tris, 0.37 g EDTA, 5 mL Triton-X filled up to 1000 mL with distilled H_2O (dH_2O), pH = 8.0), and 1 mL of the 20× proteinase K stock solution (4 mg proteinase K, 5 mL TE buffer, and 5 mL glycerol).

Pepsin. Slides were incubated in 0.025% pepsin in 0.1 mol/L HCl at 37°C for 15 minutes. After antigen retrieval slides were blocked with Teng-T (10 mmol/L Tris, 5 mmol/L EDTA, 0.15 mol/L NaCl, 0.25% gelatin, 0.05% [vol/vol] Tween-20, pH 8.0) for 30 minutes, followed by incubation overnight at 4°C with the primary antibody in PBS with 0.1% Triton X-100 and 1% bovine serum albumin. For detection of primary antibodies an avidin-biotin detection system was used. Secondary antibodies were from Dako (1:200) (anti-mouse, E0433; anti-goat, E0466; anti-rabbit, E0432), diluted in PBS with 10% human serum and incubated for 1 hour at room temperature. Slides then were incubated for 1 hour with horseradish-peroxidase (HRP)-conjugated avidin-biotin complex (DAKO, Glostrup, Denmark; K0355). For detection of some primary antibodies we used PowerVision Plus Poly-HRP detection system from Immunologic (Duiven, The Netherlands) (DPVB + 110 HRP). Peroxidase activity was detected with Sigma Fast 3.3-diaminobenzidine Tablets (Sigma, St Louis, MO; D4293). Sections were counterstained with hematoxylin, dehydrated, and mounted with Pertex (Histolab, Rockville, MD; 00801).

For staining of alkaline phosphatase, slides were dehydrated and subsequently washed 3 times for 10 minutes in NMT buffer (mix 50 mL 1 mol/L Tris pH 9, 10 mL 5 mol/L NaCl, and 25 mL 1 mol/L $MgCl_2$, and fill this up to 500 mL with dH_2O). Then slides were incubated in a Nitro blue tetrazolium/5-Bromo-4-chloro-3-indolyl phosphate (NBT/Bcip) solution for 10 minutes. For preparation of NBT/Bcip solution dissolve 1 tablet of NBT (10 mg, Sigma N5514) in 1 mL and 1 tablet of Bcip (25 mg, Sigma B0274) in 500 μL dimethylformamide. Take 17.3 μL of Bcip solution and 166.7 μL of NBT solution and mix with 5 mL NMT buffer. Slides were counterstained, dehydrated, and mounted.

Sirius Red staining was performed using a standard histochemical protocol. Slides were de-waxed, rehydrated, and incubated in Picro–Sirius red solution (Direct Red 80; Sigma Aldrich 365548, dissolved in 500 mL of saturated aqueous solution of picric acid; Sigma, P6744-1GA) for 1 hour. Slides were washed 2 times in acidified water (5 mL acetic acid [glacial] to 1 L of dH_2O), dehydrated in 3 changes of 100% ethanol, cleared in xylene, and mounted.

Immunofluorescent Staining

For immunofluorescent double staining the slides were pretreated as for immunohistochemistry (see earlier). Antibodies (Supplementary Table 1) were diluted in PBS with 0.1% Triton X-100 and 1% bovine serum albumin and slides were incubated overnight (o/n). The next day slides were washed in PBS and incubated for 2 hours in donkey-anti-rabbit 488 and donkey-anti-goat 568 (A-21206 and A-11057, respectively; Invitrogen, San Diego, CA) diluted 1:1000 in PBS with 10% serum at room temperature. Slides were washed and mounted with Vectashield (H-1000, Vector Laboratories, Burlingame, CA) with 4′,6-diamidino-2-phenylindole (10236276001; Roche).

LacZ staining

The small intestine was collected and flushed with PBS. The tissue was prefixed in cold 1% paraformaldehyde (PFA) in PBS for 2 hours. The tissue was washed 3 times for 15 minutes in PBS and incubated in an X-gal–containing solution (5 mmol/L potassium ferricyanide crystalline, 5 mmol/L potassium ferricyanide trihydrate, and 2 mmol/L magnesium chloride) in 50 mL PBS with 1.25 mL of the X-gal stock solution (20 mg/mL X-gal in dimethylformamide; Qiagen, 129931) for 3 hours at 37°C, then o/n at room temperature, shaking in the dark. The tissue was washed in PBS and fixed o/n in 4% PFA.

Supplementary Table 1. Antibodies and staining protocols

Antibody	Concentration	Company	Catalogue number	Antigen retrieval	Secondary antibody
α-Sma	1:200	Abcam, Cambridge, UK	ab5694	NaCl	Dako
α-Sma	1:100	Dako	M0851	NaCl	Fluorescent
β-catenin	1:1000	BD Biosciences	610154	Tris/EDTA	Immunologic
BrdU	1:500	Sigma	B2531	HCl and pepsin	Dako
Cd3	1:100	Dako	A0452	Tris/EDTA	Immunologic
Cd44	1:500	Serotec, Raleigh, NC	MCA1967	NaCl	Dako
Cd68	1:200	Dako	M0814	NaCl	Fluorescent
Desmin	1:100	Epitomics, Burlingame, CA	1466-1	NaCl	Dako
Desmin	1:50	Santa Cruz, Santa Cruz, CA	sc-7559	NaCl	Fluorescent
EphB2	1:50	R&D, Pleasanton, CA	AF467	NaCl	Dako
EphB3	1:50	R&D	AF432	NaCl	Dako
F4/80[a]	1:100	BMABiomedicals, Augst, Switzerland	T-2006	NaCl	Immunologic
Fibronectin	1:100	Abcam	ab23750	None	Immunologic
Lysozyme	1:400	Dako	A0099	Proteinase K	Dako
Ly6G	1:1000	BD Pharmingen, San Diego, CA	553127	Pepsin	Immunologic
Ihh[b]	1:250	Santa Cruz	sc-1196	NaCl	Dako
Pai-1	1:100	Santa Cruz	sc-8979	NaCl	Dako
pSmad1,5,8	1:200	Cell Signaling, Danvers, MA	9511	NaCl	Dako
pSmad2,3	1:250	Cell Signaling	3108	NaCl	Dako
S1004A	1:100	Neomarkers, Fremont, CA	RB-1804-A1	NaCl	Immunologic
Vimentin	1:100	Cell Signaling	3932	Tris/EDTA	Immunologic
Vimentin	1:20	Sigma Aldrich	V4630	Trypsin	Fluorescent

EDTA, ethylenediaminetetraacetic acid.

[a]For this staining an additional amplification step was performed. On day 2, after incubation with the primary antibody, we added rabbit anti-rat F(ab')2 fragments (Southern Biotech, 6130-01) 1:3000 in PBS + 10% mouse serum.

[b]The lot number of this Ihh antibody was lot #F1407. Although we were able to confirm the specificity of this antibody using intestines of conditional *Ihh* mutant mice, this does not mean that this antibody does not cross-react with Shh, because Shh is not expressed in the mouse intestine.

Generation of Dig-Labeled Probes

For mRNA in situ hybridization all probes were generated by subcloning mouse partial cDNA into a vector. A total of 1 μg of linearized plasmid DNA was transcribed in vitro using either T3 (Roche 11031163001) or T7 (Roche 10881767001) RNA polymerase in the presence of digoxin-labeled uridine 5′-triphosphate. All cDNA fragments were sequenced to verify the identity. Partial cDNA of *Lgr5* (NM_010195.2, bp 289–1274) was subcloned into the T-easy vector (Promega, Fitchburg, WI; A1360) and linearized with NcoI (antisense) and SpeI (sense). Partial cDNA of *Olfm4* (NM_001030294.1, bp 1076-1560) was subcloned into the T-easy vector and linearized with SpeI (antisense) and NcoI (sense). In vitro transcription was performed following the protocol of the commercially available RNA DIG labeling mix (Roche 1277073). The RNA pellet was dissolved in 100 μL of diethylpyrocarbonate (DEPC)-treated water and 100 μL of formamide and stored at −80°C.

Generation of ^{35}S-Uridine Triphosphate–Labeled Probes

Partial cDNA of *Ihh* (NM_010544, bp 766–2464) was subcloned into the pSportI vector and linearized with SalI (antisense) and NotI (sense). A reaction was set up with 2 μL linearized plasmid DNA (0.5 μg/mL), 2 μL 10× transcription buffer (Roche 1465384), 2 μL 0.1 mol/L dithiothreitol (Sigma-Aldrich D0632), 0.5 μL RNase inhibitor (Promega 20325507, 40 U/mL), 4 μL 2.5 mmol/L nucleotide triphosphates (NTPs) (Roche 1 140 965 [adenosine triphosphate], 1 140 922 [cytidine triphosphate], and 1 140 957 [guanosine triphosphate]), 10.5 μL sterile destilled DEPC-treated water, 2.5 μL [100 μCi] α ^{35}S-labeled uridine triphosphate (Amersham SJ 40383), and 1 μL SP6, T3, or T7 RNA polymerase (10 U/mL) (Roche 810274, 10882767, 11031163, 20 U/mL). This mixture was incubated at 37°C for 2 hours. Then 13.5 μL H_2O, 4 μL 10× DNAse buffer (Promega M198A), 2 μL RQ1-DNAse (Promega M610A), and 0.5 μL RNase inhibitor was added, followed with an additional incubation at 37°C for 20 minutes. To stop the reaction 10 μL Stop Buffer (Promega 199A) was added and the reaction mixture was incubated at 65°C for 10 minutes. The riboprobes were column purified using Chroma Spin-30, DEPC-H_2O G50 Columns (BD Biosciences, Franklin Lakes, NJ; 636087) according to the manufacturer's manual and stored in 900 μL hybridization mixture (50% formamide, 0.3 mol/L NaCl, 20 mmol/L Tris HCl [pH 8.0], 10 mmol/L $NaPO_4$ [pH 8.0],

10% dextran sulphate, sodium salt; Amersham, Piscataway, NJ; 17-0340-02), 1× Denhardt's solution (50× Denhardt's: 2.5 g bovine serum albumin, 2.5 g Ficoll, 2.5 g polyvinylpyrrolidone in 250 mL dH_2O), 0.5 mg/mL yeast transfer RNA (Invitrogen 1540-011) at −80°C.

In Situ Hybridization

dH_2O and all solutions used in the in situ protocol were treated with 300 μL/L DEPC (Brunschwig Chemie, #18835) and autoclaved before use. Paraffin-embedded tissue was sectioned (8 μm) and mounted on SuperFrost Plus microscope slides (Menzel-Gläser, Braunschweig, Germany; J1800AMNZ). Tissue slides were deparaffinated, rehydrated, and post-fixed in 4% paraformaldehyde in PBS on ice for 20 minutes. After rinsing the slides twice in PBS for 5 minutes, sections were overlayed with 500 μL of 40 μg/mL proteinase K (Roche 161519) in 50 mmol/L Tris HCl (pH 8.0), 5 mmol/L EDTA, and incubated for 7.5 minutes. Slides were washed in PBS for 5 minutes and refixed in 4% paraformaldehyde in PBS on ice for 5 minutes. Slides were washed shortly in PBS and dH_2O and placed in 0.1 mol/L triethanolamine (Fluka, St Louis, MO; 90279) on a magnetic stirrer. While stirring 625 μL of acetic anhydride (Sigma A-6404) was added and left for 10 minutes. Slides were washed with PBS for 5 minutes each. Slides were dehydrated and air dried. Probe stocks were diluted 100× in hybridization mixture (see earlier) and heated for 2 minutes at 80°C and placed on ice. The probe mix was brought to room temperature and spread evenly over the tissues and covered with a coverslip. As negative controls, sense probes were applied. Slides were incubated overnight in a hybridization oven at 55°C together with tissues soaked in 50% formamide and 5× saline sodium citrate (SSC; 43.8 g NaCl, 22 g sodium citrate in 1 L H_2O, pH 6.4) to prevent dehydration of the tissues. The next day slides were washed in 5× SSC at room temperature, followed by a high-stringency wash in 50% formamide, 2× SSC at 55°C. Subsequently, slides were washed in STE buffer (0.5 mol/L NaCl, 10 mmol/L Tris HCl [pH 8], 5 mmol/L EDTA) 1 time at room temperature and 3 times at 37°C for 10 minutes each. Slides were treated with 20 μg/mL RNase (Sigma R6513) in 50 mL STE at 37°C for 30 minutes, washed with STE at 37°C for 15 minutes, followed by another high-stringency wash in 50% formamide, 2× SSC at 70°C for 30 minutes. Slides were washed with 2× SSC at room temperature for 15 minutes. After this step slides were dehydrated, air-dried, and exposed to hyperfilm (Amersham Biosciences RPN6K) to determine the exposure time to LM-1 solution. For autoradiography slides were treated with hypercoat LM-1 emulsion (Amersham RPN40) according to the manufacturer's instructions.

RNA Isolation and cDNA Synthesis

For isolation of RNA an RNeasy kit from Qiagen (74104) was used. The proximal part of the duodenum was homogenized, in buffer RLT, using a rotor-stator homogenizer. Homogenates were spinned at 14,000 RPM and supernatant was used for RNA isolation, following the Qiagen protocol. Obtained RNA was treated with DNAse-I (Promega M610A) in 10× DNAse buffer (Promega M198A) for 30 minutes at 37°C. The reaction was stopped by adding Stop Solution (Promega M199A) and incubating the solution for 5 minutes at 65°C. cDNA was synthesized from a mixture of 100 ng/μL RNA, first-strand buffer (Invitrogen y02321), deoxynucleoside triphosphates (Invitrogen 18427-013), random hexamers (Promega #C1181), RNAse inhibitor (Promega 23766810), and Superscript II Reverse Transcriptase (Invitrogen 18064-014). This mixture was incubated at 25°C for 7 minutes, 42°C for 60 minutes, 95°C for 3 minutes, and cooled to 10°C.

Quantitative RT-PCR

Quantitative RT-PCR was performed using a mix of 5 μL Sybr Green Mastermix (Roche, #04707516001), 3 μL H_2O, 1 μL primer mix, and 1 μL diluted cDNA (1:4). Primers were all pre-optimized primers from Qiagen; *Bmp2* (QT01054277), *Bmp4* (QT00111174), *Bmp7* (QT00096026), *Gapdh* (QT01658692), *Gli1* (QT00173537), *Goosecoid* (QT00095221), *Hhip* (QT00147518), *Id1* (QT01743756), *Id2* (QT01038870), *Id3* (QT00248185), *Id4* (QT00324352), *Ihh* (QT00096215), *Inhα* (QT00246953), *Inhβa* (QT00101563), *Inhβb* (QT00245259), *Inhβc* (QT00091651), *Inhβe* (QT00250803), *Pai-1* (QT00154756), *Ptch1* (QT00149135), *Ptch2* (QT01763783), *Tgfβ1* (QT00145250), *Tgfβ2* (QT00106806), and *Tgfβ3* (QT00166838). A LightCycler 480 Instrument II (384-well version) from Roche (#05015243001) was used for the quantitative RT-PCR assay. Concentrations were divided by the amount of *Gapdh* in each sample. Expression of *Gapdh* was distributed equally between the wild-type and the *Ihh* mutant mice.

Intestinal Permeability Assays

Ussing chamber experiments. Ussing chamber experiments were performed as previously described.[1] Segments of tissue of the distal small intestine were opened, cut, and immersed in Meyler's buffer (128 mmol/L NaCl, 4.7 mmol/L KCl, 1.3 mmol/L $CaCl_2 \cdot 2H_2O$, 20.2 mmol/L $NaHCO_3$, 0.4 mmol/L $NaH_2PO_4 \cdot H_2O$, 0.33 mmol/L $Na_2HPO_4 \cdot 2H_2O$, 1 mmol/L $MgCl_2 \cdot 6H_2O$, 10 mmol/L HEPES, 10 mmol/L D-glucose). Within 15 minutes, the tissue was mounted in Ussing chambers (World Precision Instruments, Berlin, Germany) with serosal and mucosal areas exposed to 2 mL of circulating oxygenated Meyler's buffer and maintained at 37°C. Short-circuit current (in $\mu A/cm^2$), a measure of net active ion transport, was recorded by a computer connected to a voltage-clamp system. After 15 minutes, HRP was added to the luminal buffer at a final concentration of 10 μmol/L. After 30, 60, and 90 minutes, samples (300 μL) were taken on the serosal side and replaced with fresh buffer. The enzymatic activity of HRP was measured using OPD (Sigma, P5412) as substrate.

Everted Gut Sac

Intestinal permeability was assessed by measuring permeability to HRP in isolated segments of ileum as previously described.[2–4] In short, 8-cm segments of the distal ileum were washed, everted, and filled with 1 mL of Meyler's buffer (see earlier) and ligated at both ends. The filled segment was incubated in Tris buffer containing 40 mg/mL of HRP (Sigma). After incubation at room temperature for 45 minutes, segments of ileum were removed from the buffer, and the content was carefully collected in a 1-mL syringe. HRP activity was measured spectrophotometrically at 405 nm after addition of tetramethylbenzidine (TMB) as substrate for HRP.

Fluorescein Isothiocyanate–Labeled Dextran Uptake in the Blood

The uptake of fluorescein isothiocyanate–labeled dextran in blood was assessed as previously described.[5,6] Mice were administered 0.6 mg/g body weight of an 80 mg/mL solution of fluorescein isothiocyanate–dextran (FD-4; Sigma) per gavage. After 4 hours peripheral blood was collected. A standard curve was generated from dilutions of fluorescein isothiocyanate–dextran in PBS. Absorption of 50 μL serum or standard was measured in a fluorometer at 488 nm.

References

1. van der Zanden EP, Snoek SA, Heinsbroek SE, et al. Vagus nerve activity augments intestinal macrophage phagocytosis via nicotinic acetylcholine receptor alpha4beta2. Gastroenterology 2009;137:1029–1039.
2. Carter EA, Harmatz PR, Udall JN, et al. Barrier defense function of the small intestine: effect of ethanol and acute burn trauma. Adv Exp Med Biol 1987;216A:829–833.
3. Luyer MD, Buurman WA, Hadfoune M, et al. Pretreatment with high-fat enteral nutrition reduces endotoxin and tumor necrosis factor-alpha and preserves gut barrier function early after hemorrhagic shock. Shock 2004;21:65–71.
4. de Haan JJ, Lubbers T, Hadfoune M, et al. Postshock intervention with high-lipid enteral nutrition reduces inflammation and tissue damage. Ann Surg 2008;248:842–848.
5. Karhausen J, Furuta GT, Tomaszewski JE, et al. Epithelial hypoxia-inducible factor-1 is protective in murine experimental colitis. J Clin Invest 2004;114:1098–1106.
6. Kaser A, Lee AH, Franke A, et al. XBP1 links ER stress to intestinal inflammation and confers genetic risk for human inflammatory bowel disease. Cell 2008;134:743–756.

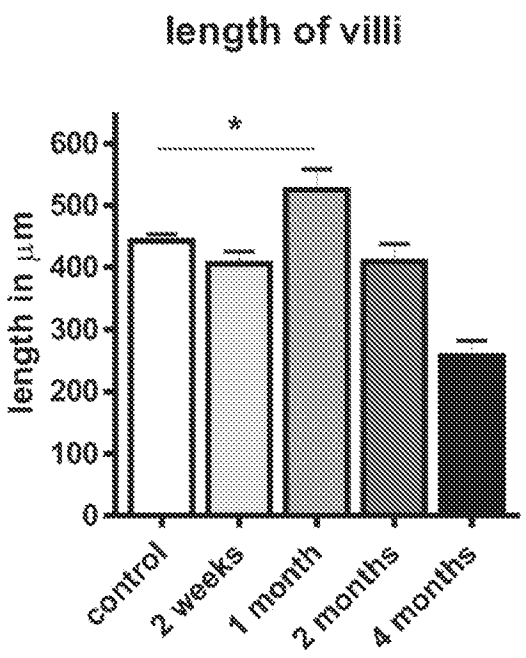

Supplementary Figure 1. One month after recombination a mild transient increase in villus length was found (443 μm in the wild-type mice vs 525 μm in the mutant mice; $^*P < .05$).

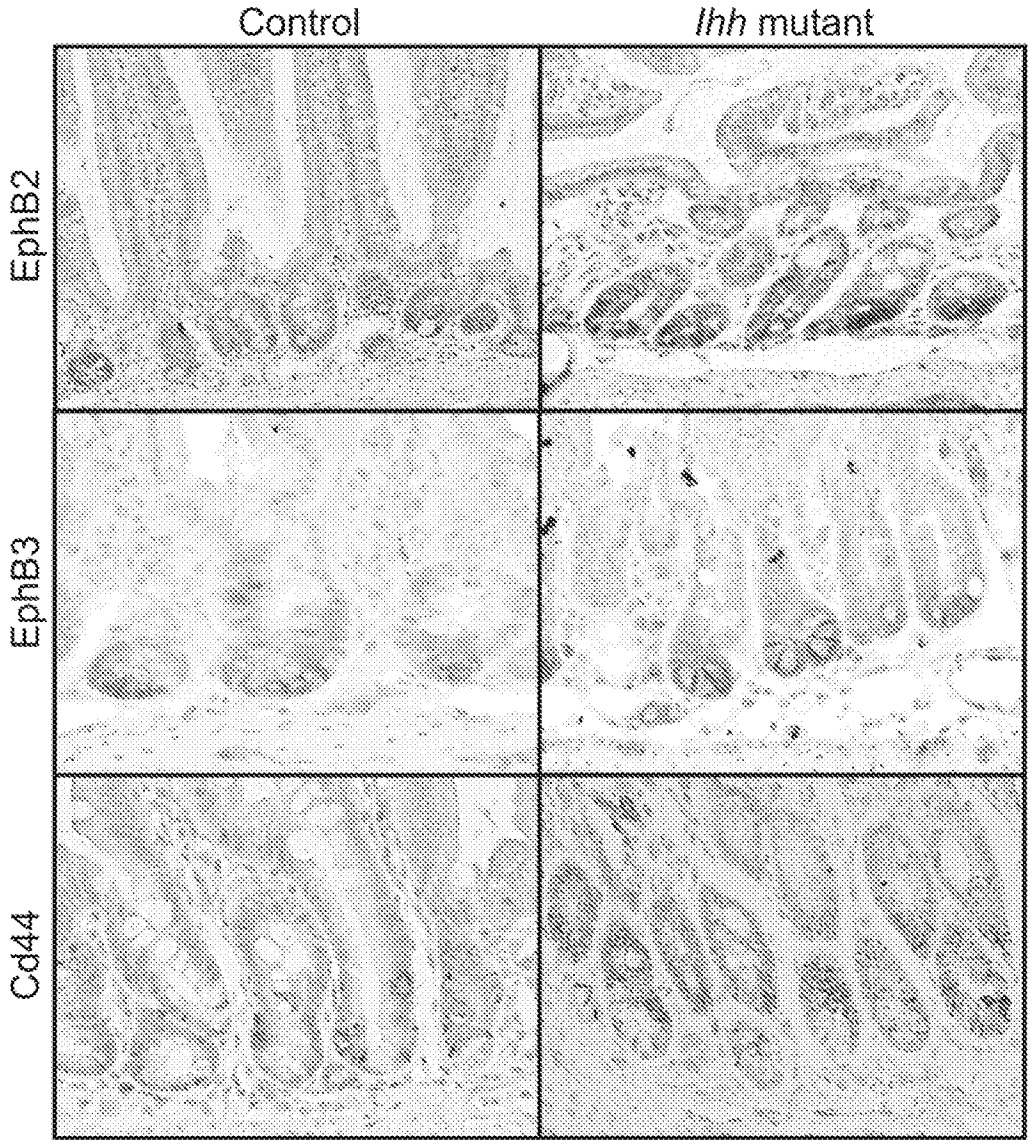

Supplementary Figure 2. EphB2, EphB3, and Cd44, targets of Wnt signaling were all up-regulated in the *Ihh* mutant mice 1 month after recombination. Original magnification, 400×.

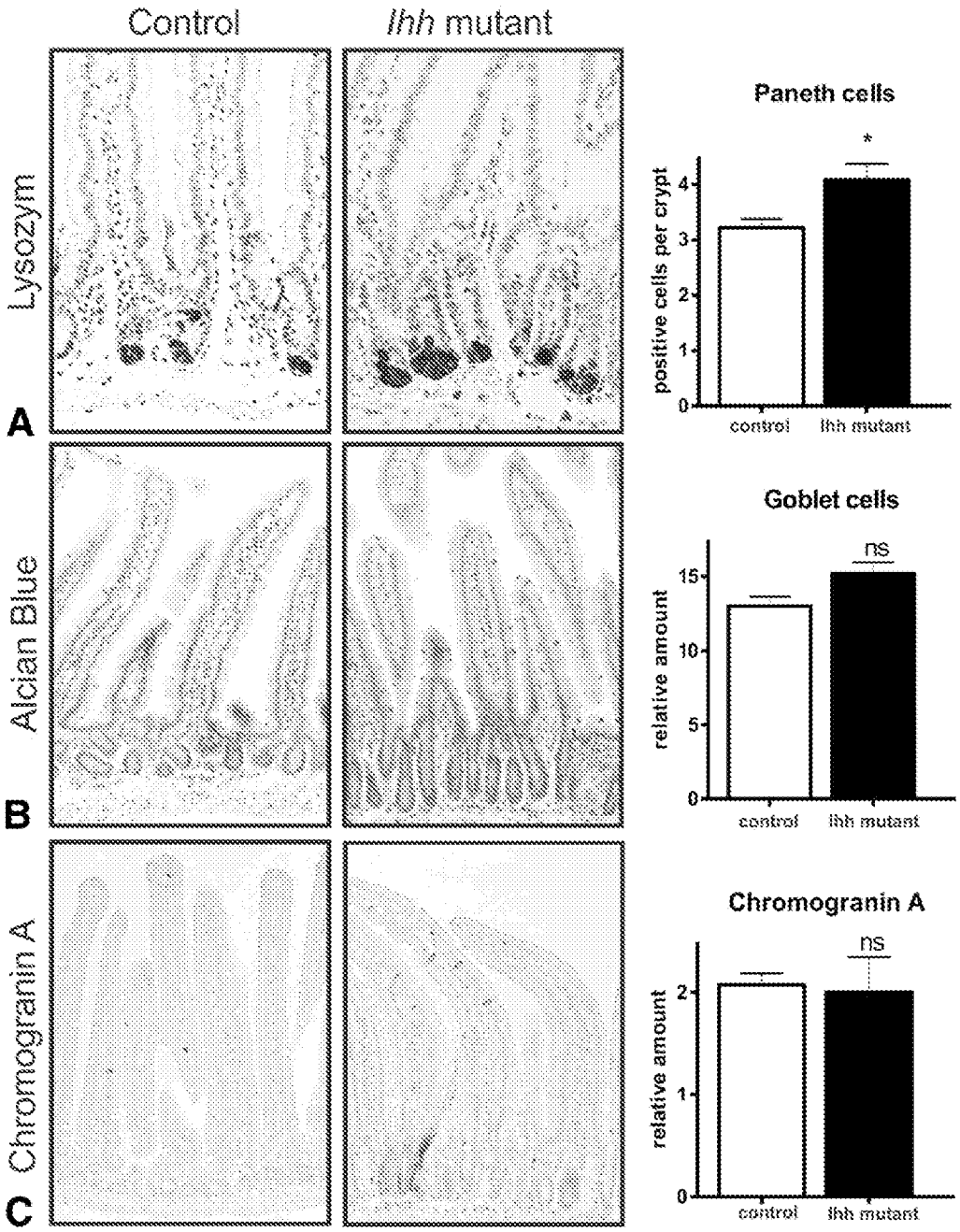

Supplementary Figure 3. (*A*) Immunohistochemistry for lysozyme, a Paneth cell marker, 1 month after recombination. A modest increase in lysozyme-positive cells was observed at the base of the crypts of mutant mice 1 month after recombination. We found 3.2 positive cells per crypt (n = 8) versus 4.1 positive cells per crypt in the Ihh mutant mice (n = 5; *P = .015). (*B*) Immunohistochemistry for Alcian Blue, a Goblet cell marker, 1 month after recombination. The relative increase in Goblet cells was not significant (P = .06; n = 5 for both control and mutant groups). (*C*) Immunohistochemistry for chromogranin A, a marker for enteroendocrine cells, 1 month after recombination. No difference was found in the relative amount of enteroendocrine cells between the control and the mutant mice (P = .8; n = 5 for both groups). Original magnification, 200×.

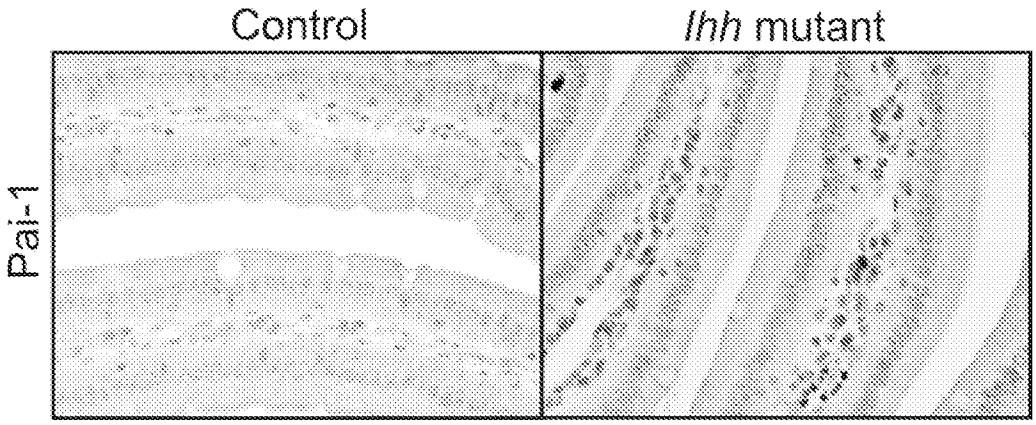

Supplementary Figure 4. Immunohistochemistry for Bmp signaling target Pai-1 showed increased levels of Pai-1 in the mesenchyme of mutant mice 1 month after recombination. Original magnification, 400×.

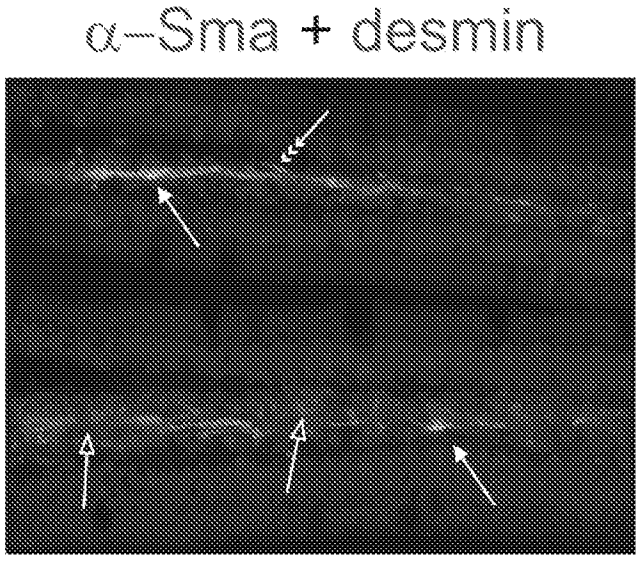

Supplementary Figure 5. An immunofluorescent double staining for α-Sma and desmin in control mice. The double staining showed that most cells in the villus core were either smooth muscle cells (desmin single-positive cells, *open arrows*) or smooth muscle precursor cells (desmin–α-Sma double-positive cells, *closed arrows*). The *triple arrow* indicates an α-Sma single-positive cell. Original magnification, 400×.

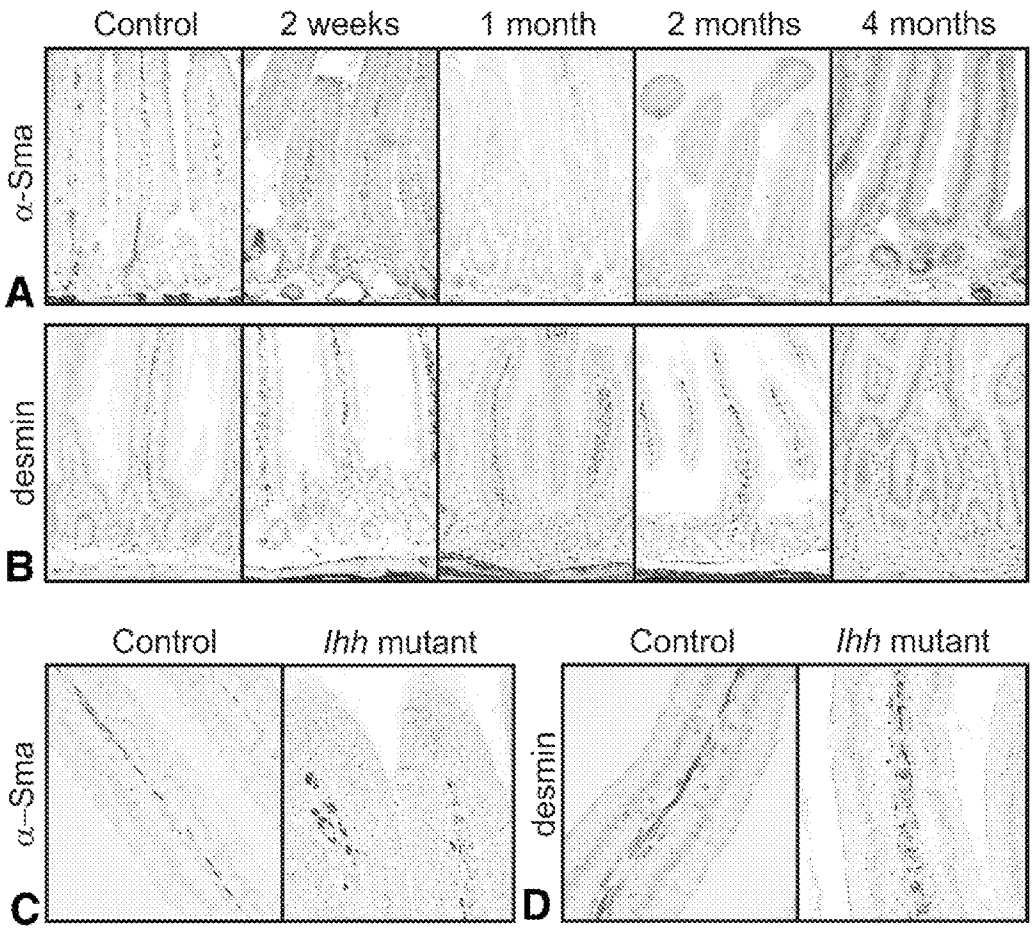

Supplementary Figure 6. Loss of smooth muscle cells from the villus core in *Ihh* mutant mice. (*A*) α-Sma–positive cells were reduced in number at 1 month after recombination and had disappeared at the 2- and 4-month time points. (*B*) Desmin-positive cells were present in the villi until 2 months after recombination and disappeared at 4 months after recombination. (*C* and *D*) α-Sma and desmin-positive cells had an elongated appearance in the control mice. In the *Ihh* mutant mice, 1 month after recombination, the remaining α-Sma–positive cells and the desmin-positive cells had lost their elongated structure and seemed to roll up into a sphere-like shape. Original magnifications, (*A* and *B*) 200× and (*C* and *D*) 400×.

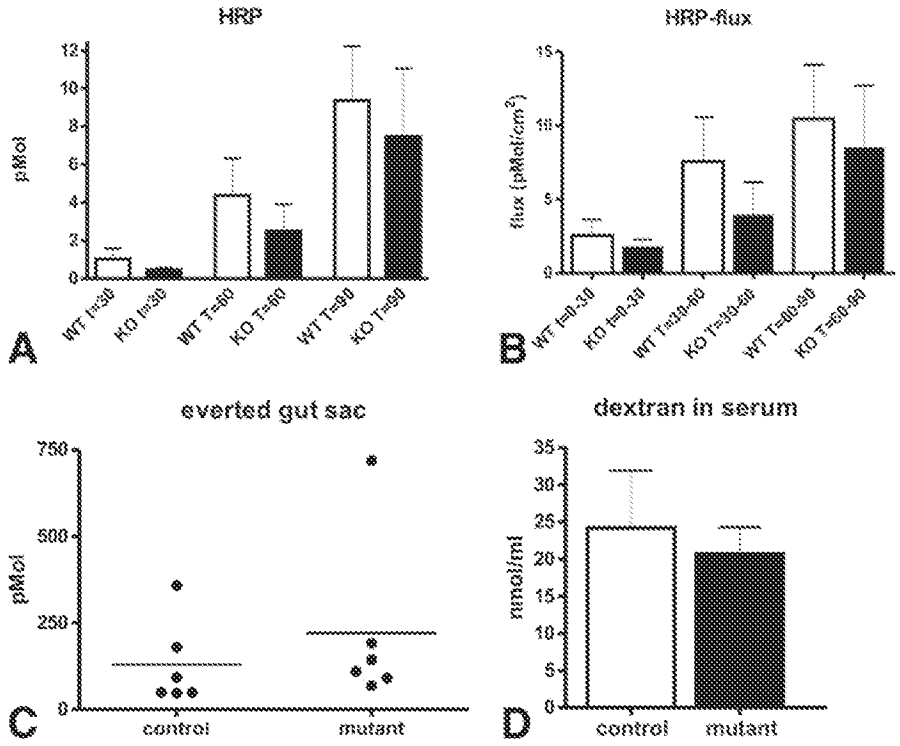

Supplementary Figure 7. No difference in barrier function between control mice and *Ihh* mutant mice 1 month after regeneration. (*A*) Ussing chamber experiment measuring the absolute amount of HRP passing through a piece of small intestine in 30, 60, and 90 minutes and (*B*) the average flux between the different time points. (*C*) Amount of HRP going from the luminal to the serosal side in an everted gut sac. (*D*) Levels of fluorescein isothiocyanate–labeled dextran measured in the serum 4 hours after administration per gavage.

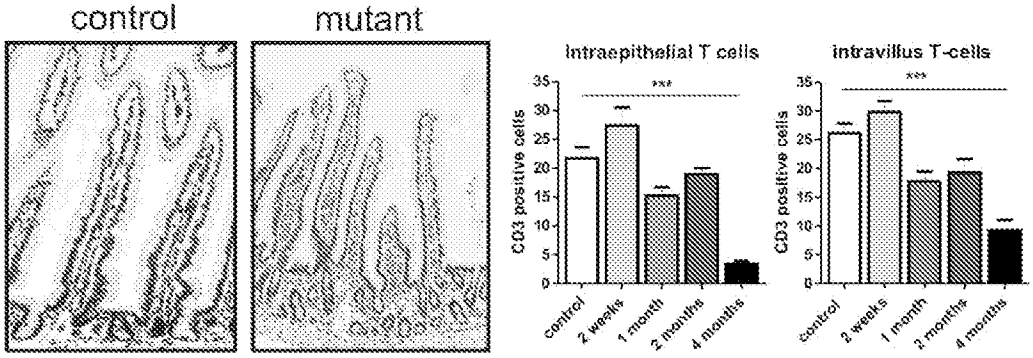

Supplementary Figure 8. The number of Cd3-positive intraepithelial lymphocytes decreased from 21.7 cells in control mice (n = 8) to 3.5 cells in mutant mice 4 months after recombination (n = 4; $^{***}P < .001$) and the number of Cd3-positive cells in the villus core decreased from 26.1 positive cells in control mice (n = 8) to 9.3 positive cells in the mutant mice 4 months after recombination (n = 4; $^{***}P < .001$). Original magnifications, (*A*) 400× and (*B*) 200×.